Arabian Journal of Chemistry (2021) **14**, 103114

King Saud University

Arabian Journal of Chemistry

www.ksu.edu.sa
www.sciencedirect.com

ORIGINAL ARTICLE

Adsorption and corrosion of renewable inhibitor of *Pomelo* peel extract for mild steel in phosphoric acid solution

Bi-lan Lin [a,*], Jun-jie Shao [a], Yu-ye Xu [b,*], Yi-ming Lai [a], Zhong-ning Zhao [a]

[a] *School of Material Science and Engineering, Xiamen University of Technology, No.600 Ligong Road, Jimei District, Xiamen, Fujian Province, China*
[b] *College of Civil Engineering, Huaqiao University, No.668 Jimei Avenue, Jimei District, Xiamen, Fujian Province, China*

Received 24 December 2020; accepted 4 March 2021
Available online 12 March 2021

KEYWORDS

Metal corrosion;
Plant extract;
Acid corrosion;
Electrochemical measurements;
Renewable inhibitor;
Adsorption

Abstract *Pomelo* peel extract (*PPE*) was evaluated as green and renewable corrosion inhibitor for mild steel in 1.0 mol/L H_3PO_4 solution. The inhibition behaviour was studied using mass loss, potentiodynamic polarization (PDP) and electrochemical impedance spectroscopy (EIS) measurements. The chemical structure of *PPE* was investigated using Fourier transform infrared (FT-IR) and ultraviolet-visible (UV–vis) spectroscopy. The corrosion morphology of mild steel was analysed via scanning electron microscopy (SEM). The adsorption thermodynamics and kinetics was discussed. The results show that *PPE* confers an acceptable long-term effect (inhibition efficiency of 95.0% and 92.8% for corroding 23 h and 224 h in the presence of 5.0 g/L *PPE* inhibitor) and functions as a mixed inhibitor. The adsorption of *PPE* on mild steel simultaneously follows the Langmuir, El-Awady and Temkin isotherms at 35, 45 and 55 °C. *PPE* is mixed adsorption dominated with physical adsorption at room temperature or with higher *PPE* concentrations. *PPE* possesses many polar functional groups such as hydroxyl, carbonyl and hetero-aromatic rings. The inhibition mechanism is closely related to these polar groups, as is the surface coverage of steel.

1. Introduction

Metal corrosion is an aggressive and detrimental electrochemical process. The control of metal corrosion has attracted considerable attention in modern times (Aslam et al., 2020; Popoola, 2019). Given the simplicity of the corrosion process and its widespread and costly impact, corrosion inhibitors have been extensively used in pickling, extraction and refining operations in oil and gas, machinery, chemical industry,

* Corresponding authors.
E-mail addresses: linbilan@xmut.edu.cn (B.-l. Lin), yuyexu@hqu.edu.cn (Y.-y. Xu).

Peer review under responsibility of King Saud University.

Production and hosting by Elsevier

https://doi.org/10.1016/j.arabjc.2021.103114
1878-5352

energy, infrastructure, civil engineering and associated industries (Fateh et al., 2020; Verma et al., 2018).

In 1860, a patented formula for a corrosion inhibitor based on a mixture of syrup and vegetable oil was described by Baldwin. In the 20th century, the constituents of corrosion inhibitors gradually changed from natural plant extracts to mineral raw materials, and inhibitor preparations were based on large-scale artificial syntheses employing organic compounds, organic salts and inorganic salts (Saei et al., 2017; Xhanari and Finšgar, 2019). However, many corrosion inhibitors, such as chromate, mercury salts and imidazole, are hazardous, harmful, expensive and difficult to biodegrade. Likewise, phosphate inhibitors are likely to cause eutrophication of water and scale formation in recirculating cooling water systems (Fang et al., 2020). Corrosion inhibitors may be extracted from plants and have the advantages of wide availability, relatively low cost, low toxicity or non-toxic, high efficiency and ease of degradation, and thus have become one of the main directions for developing green and renewable corrosion inhibitors (Alrefaee, et al., 2020; Harb, et al., 2020; Raja and Sethuraman, 2008).

Many plant extracts contain alkaloids, saponins, tannic acids, sugars, amino acids and aromatics. Their electronic structures invariably possess π electrons, lone-pair electrons associated with O, N and other hetero-atoms on non-ligands, have good corrosion inhibition effects, thus they may behave similarly to conventional organic compound based corrosion inhibitors (Caio et al., 2019; Oguzie et al., 2010). Recently, many studies have been conducted on the extraction of corrosion inhibitors from the stems, leaves, flowers and seeds of plants, peels of fruit, marine algae and crops (Dehghani et al., 2020; Fadhil et al., 2020; Garai et al., 2012).

In the process of acid pickling, acid leaching and oil well acidification, the acidic media will corrode the metal structures. The use of corrosion inhibitors is one of the most practical methods to prevent the excessive consumption of metals. The acid media are usually HCl, H_2SO_4, H_3PO_4, organic acids, etc. Recently, research on the use of plant extracts as corrosion inhibitors in acid media mainly involves HCl, followed by H_2SO_4, while studies on H_3PO_4 and organic acids have been limited. Among the metals, reselooph on carbon steels is dominant, while studies on nonferrous metals and stainless steel are relatively few. Extracts of *Pimenta dioica* leaf (Anupama et al., 2015), *Retama monosperma* (*L.*) *boiss*. seed (Hamdani et al., 2015), *Ficus tikoua* leaf (Wang et al., 2019), *Eriobotrya japonica lindl* leaf (Nikpour et al., 2019), *Aquilaria subintergra* leaf (Sin et al., 2017), *Prunus dulcis* peel (Pal et al., 2019), *Glycyrrhiza glabra* leaf (Alibakhshi et al., 2018), *Parsley* (*Petroselium sativum*) leaf (Benarioua, et al., 2019), *Musa paradisica* peel (Ji, et al., 2015), *Borage* flower (Dehghani et al., 2019), *Sargassum muticum* (Nadi et al., 2019), Sunflower seed (Hassannejad and Nouri, 2018), *Tithonia diversifolia* flower (Divya et al., 2019) and *Xanthium strumarium* leaf (Khadom et al., 2018) have been shown to exhibit good inhibition effect on carbon steel in HCl medium. Extracts of *Citrus aurantium* leaf (Hassan et al., 2016), *Nauclea latifolia* leaf, bark and roots (Uwah et al., 2013), and *litchi* (*Litchi Chinensis*) peel (Singh et al., 2019) gave acceptable inhibition for carbon steel in H_2SO_4 medium. Extracts of *Spondias mombin L.* (Obi-Egbedi et al., 2015), *Lasienthera africanum* (Fayomi et al., 2018) and *Dryopteris cochleata* leaf (Nathiya and Raj, 2017) were shown to impede the corrosion of aluminium alloy in acid medium.

The inhibition effects of the various plant extracts show differences in performance, leading to different adsorption isotherms on the metal surface. In acid media, most plant extracts such as *Pimenta dioica* leaf (Anupama et al., 2015), *Retama monosperma* (*L.*) *boiss*. seed (Hamdani et al., 2015), *Ficus tikoua* leaf (Wang et al., 2019), *Glycyrrhiza glabra* leaf (Alibakhshi et al., 2018) and *Citrus aurantium* leaf (Hassan et al., 2016) followed the Langmuir adsorption isotherm. However, extract of *Dryopteris cochleata* leaf on aluminium alloy obeyed the Freundlich isotherm (Nathiya and Raj, 2017); extracts of *Nauclea latifolia* leaf, bark and root conformed to the El-Awady isotherm (Uwah et al., 2013); extract of *Tithonia diversifolia* flower obeyed both the Langmuir and Temkin isotherms (Divya et al., 2019).

Besides the adsorption isotherms on the metal surface, the adsorption model and the inhibition mechanism for different plant extracts may also be different. The adsorption model includes physical adsorption, chemical adsorption and mixed adsorption. The inhibition mechanism includes the anode type, the cathode type and the mixed type. According to the literatures (Alibakhshi et al., 2018; Dehghani et al., 2019; Hussin et al., 2016), most plant extracts function as mixed inhibitors, some act as the cathode type while a few others function as the anode type. The inhibition and adsorption mechanism of *Glycyrrhiza glabra* leaf extract on carbon steel in 1.0 mol/L HCl were investigated through PDP, EIS, atomic force microscopy (AFM) and contact angle tests, as well as molecular dynamics, Monte Carlo and quantum mechanics simulations (Alibakhshi et al., 2018). The results showed that the *Glycyrrhiza glabra* leaf extract was a mixed inhibitor, and the inhibition efficiency was 88% for a 0.8 g/L extract after immersion for 24 h. The active components in the extract were adsorbed on steel due to the donor- acceptor interactions. An extract of *Retama monosperma* (*L.*) *boiss*. seed was used as a corrosion inhibitor for carbon steel in 1.0 mol/L HCl (Hamdani et al., 2015). The results for PDP, EIS and SEM indicated that the extract was a mixed inhibitor dominated by physical adsorption, and the inhibition efficiency was up to 94% when the extract concentration was 0.4 g/L. The inhibition mechanism for *Zizyphus Lotuse* extract on copper in 1.0 mol/L HCl was investigated by gravimetric, PDP, EIS, SEM, EDS, AFM and FT-IR (Jmiai, et al., 2018). The studies showed that the inhibition efficiency was 93% and the extract was a cathodic inhibitor. An extract of *Borage* flower on mild steel exhibited mixed adsorption in HCl solution and functioned as a mixed inhibitor with the main inhibition of the anode type (Dehghani et al., 2019). An extract of *Sargassum muticum* was chemically adsorbed on carbon steel and functioned as a mixed inhibitor (Nadi et al., 2019).

The differences in the extraction methods, extraction solvents and plant parts invariably leads to differences in the amounts and types of components in extract, hence leading to different inhibition efficiencies. Also the same plant extract for different metals would also result in the different inhibition efficiency. Ethanol and water were examined as extraction solvents for *Dryopteris cochleata* leaf and *Borassus flabellifer* dust; both extracts with ethanol as solvent offered an enhanced inhibition effect for aluminium alloy relative to those for water (Nathiya and Raj, 2017, 2019). Compared with water, methanol was more effective for extraction of active constituents from *Prunus dulcis* peel, which contributed to higher inhibition efficiency (Pal et al., 2019). However, the inhibition efficiency

of *Tinospora crispa* extracted with water was higher than that with acetone (Hussin et al., 2016). The inhibition of an extract of *Nauclea latifolia* decreased in the following order: root > leaf > bark; and physical adsorption was the primary adsorption model for all extracts (Uwah et al., 2013). The inhibition effect of unripened banana peel extract was reported to be greater than that of ripened banana peel (Ji et al., 2015). The inhibition efficiencies for *Griffonia simplicifolia* extract in 1.0 mol/L HCl for mild steel, X80 and J55 were 91.7%, 79.8% and 75.4%, respectively (Ituen et al., 2017).

Pomelo is a *Rutaceae* plant and an evergreen tree. The leaves are large and thick, and the fruit peel is thick. The fruit can be used raw or in food processing. The peel can be used as preserves. Aromatic oil can be extracted from the flowers, leaves and peel. *Pomelo* has a long culture history in China and Southeast Asian countries, there being widespread planting, an abundance of crops and a low price. *Pomelo* peel contains mainly flavonoids, sterols, fatty acids, sugars, insulin, limonin, neohesperidin and so on, and it is rich in heterocyclic, hydroxyl, carbonyl and other active groups (Mhiri et al., 2016; Zhang and Zhao, 2018). These groups have excess negative charge and can donate electrons to the empty 3*d* orbitals of metals, thus they can be readily adsorbed on metallic surfaces and form a protective film, thus slowing down the corrosion of the metal (Sun, et al., 2017; Yee, et al. 2020). Except for a small amount of *Pomelo* peel being used for medicinal purposes and for fruit preservation, most of the peel is discarded. Clearly, in-depth studies on the extraction of active chemical components from *Pomelo* peel is warranted, including the use of *Pomelo* peel extracts for corrosion protection of metal given the important potential economic and social benefits for development of rural economies and comprehensive utilization of natural resources.

Phosphoric acid has been widely used in fertilizer production, oil exploitation and surface treatment processes of metallurgical industry (Dkhireche et al., 2020; Gunasekaran and Chauhan, 2004). Due to a ternary moderately-strong acid, phosphoric acid also has serious corrosion effect on metal surface. Phosphoric acid will undergo three-stage ionization in solution, resulting in complex phosphate anions and complicated corrosion system. And there is an adsorption competition between phosphate anions and inhibitor molecules on metal surface (Belghiti et al., 2019; Messali et al., 2017; Taha et al., 2020). Compared with hydrochloric acid and sulfuric acid, the adsorption of corrosion inhibitor on metal in phosphoric acid solution is more complicated. Research of organic or extract inhibitors for metal in phosphoric acid solution is relatively rare (Anaee et al., 2019; El-Ibrahimi et al., 2020; Ismail and Farag, 2020). At present, the concentration of phosphoric acid also is not consistent, such as 0.5 mol/L (Anaee et al., 2019), 1.0 mol/L (Boudalia et al., 2019; Xu et al., 2019; Yaro et al., 2013), 2.0 mol/L (Belghiti et al., 2019; Dkhireche et al., 2020; Faydy et al., 2020; Ismail and Farag, 2020), 8.0 mol/L (Taha et al., 2020). Li et al. (2009) found that the effect of cresol red inhibitor on the corrosion rate of cold rolled steel was related to the concentration of phosphoric acid ranged from 1 to 10 mol/L.

In this paper, *Pomelo* peel extract (*PPE*) was used as a green and renewable corrosion inhibitor for mild steel in 1.0 mol/L H_3PO_4 solution. The inhibition performance was studied based on mass loss and electrochemical measurements. The chemical structures of the extract were studied using UV–vis and FT-IR spectroscopy, and adsorption thermodynamic and kinetic studies on mild steel by the active constituents in *PPE* were undertaken.

2. Experimental procedure

2.1. PPE extraction

The fresh *Pomelo* was purchased from Jimei farmers' market in Xiamen of China, and the variety was *Pinghe Pomelo* which was productive locally. The fresh *Pomelo* peel was washed, left overnight and then dried in an oven at 80 °C before finally being crushed in a grinder. The coarse particles were removed using a 60-mesh sieve. The *Pomelo* peel powder was dissolved in 80% (*vol*%) aqueous ethanol solution, and then extracted ultrasonically at 40 °C for 4 h. The undissolved residue was removed by vacuum filtration. The filtrate was concentrated by a vacuum rotary evaporator (model RE-52AA, Shanghai Yarong Biochemical Instrument Co., Ltd., China), and the aqueous ethanol solution was recovered. Finally, the concentrated solution was dried in an oven at 80 °C to obtain the solid *PPE*.

2.2. Materials

The tested sample was mild steel (Fujian Sansteel (Group) Co., Ltd., China), and the chemical composition (*wt*%) was: 0.13C, 0.02Si, 0.38 Mn, 0.014P, 0.031S, and the balance being Fe.

2.3. Corrosion medium preparation

The corrosion medium was 1.0 mol/L H_3PO_4 solution which was diluted from 85 *wt*% phosphoric acid (Xilong Science Co., Ltd., China). The concentration of *PPE* in H_3PO_4 solution was in the range from 0 to 10.0 g/L.

2.4. Mass loss measurements

The size of the mild steel sample used in mass loss tests was 50 mm × 40 mm × 2 mm. All faces of the sample were polished consecutively with a series of waterproof sandpapers (240#, 400#, 600#, 800#, 1000# and 1200#). The sample faces were rinsed with distilled water, scrubbed with alcohol, rinsed with distilled water and dried in cool air.

The initial mass of the above sample before corrosion (w_0) was measured. The accuracy was 0.1 mg. Then each sample was suspended alone in a 250 mL solution at specified temperatures for 8 h. The corroded sample was then cleaned with detergent, rinsed with distilled water and dried with cool air. The corresponding corroded sample (w) was weighed. The mass loss was calculated. The average corrosion rate (v) for mild steel and the corrosion inhibition efficiency (η) of *PPE* were calculated as follows

$$v = \frac{w_0 - w}{S \cdot t} \tag{1}$$

$$\eta(\%) = \frac{v^0 - v^{inh}}{v^0} \times 100\% \tag{2}$$

where w_0 and w are the mass of the mild steel sample before and after corrosion; S is the total surface area of the corroded

sample; t is the corrosion time and was 8 h in this study. v^0 and v^{inh} are the corrosion rates for mild steel without and with *PPE* inhibitor, respectively. To ensure the reliability of the results, five parallel samples were taken for each process and the average was calculated.

2.5. Electrochemical measurements

The dimensions of the mild steel sample used in electrochemical measurements were 1.0 cm × 1.0 cm × 0.2 cm, and the working area was 1.0 cm^2. The working surface was rubbed carefully with waterproof sandpaper (1200#) and rinsed successively with distilled water, acetone and distilled water.

All electrochemical measurements were performed at room temperature using an electrochemical workstation (model CHI604E; Shanghai Chenhua Instrument Co., Ltd., China). A conventional 3-electrode system featuring working, auxiliary and reference electrodes was used. The mild steel sample was used as the working electrode. A saturated calomel electrode (SCE) and a Pt electrode served as the reference electrode and counter electrode, respectively. The electrochemical measurements were implemented after the open circuit potential (OCP) of the corrosion system was stabilized.

The EIS measurements were obtained at OCP for the frequency range from 100 kHz to 0.01 Hz. The AC signal amplitude was 10 mV. The impedance data were fitted with Zview software.

The PDP experiment was conducted after the sample had been immersed for 1 h in the corrosive medium with the corrosion system being stable. The polarization range was ±300 mV vs. OCP, and the scan rate (from cathode to anode) was 1 mV/s.

To ensure the repeatability and the reliability of the electrochemical measurements, three parallel tests were conducted for each experimental condition. Here, the change trend of OCP with time under three parallel conditions should be similar, and the deviation of the final stable OCP value should be less than 20 mV. The shape of EIS diagrams and PDP curves under three parallel processes must be consistent, and the difference of the corresponding parameters should be less than 10%. In the process of experiment, it is found that the reliability of electrochemical test results in this paper is good.

2.6. UV–Vis and FT-IR spectroscopy measurements

A solution containing 1.0 mol/L H_3PO_4 and 5.0 g/L *PPE* was divided into two portions. The polished and cleaned mild steel sample was immersed in one of the solution at room temperature for 24 h. The two solutions were then diluted and analysed by UV–Vis spectrophotometry (model UV-2700; Shimadzu, Japan). The wavelength range was from 190 to 800 nm. The scanning interval was 1 nm. Distilled water was used as the reference solution.

The fully dried *PPE* and the *PPE* adsorption film which was formed on mild steel surface and was subsequently been scraped off were mixed with KBr, respectively. The samples were thoroughly mixed and ground in an agate mortar, and then the ground powders were pressed. The IR absorption spectra were measured at room temperature by a FT-IR spectrometer (model ALPHA; Bruker, Germany). The wavenumber range was from 400 to 4000 cm^{-1}.

2.7. Corrosion morphology analysis

The polished and cleaned mild steel samples were immersed in 1.0 mol/L H_3PO_4 solution containing different concentrations of *PPE* for 1 h, then rinsed with distilled water and dried with cool air. The corrosion morphology was characterized using scanning electron microscopy (SEM) (model EVO 18; Zeiss, Germany).

3. Results and discussion

3.1. Corrosion rate from mass loss test

The effects of the *PPE* concentration (C_{inh}) and the temperature of the corrosion medium on corrosion rate of mild steel (v) and inhibition efficiency of *PPE* (η) in 1.0 mol/L H_3PO_4 solution are illustrated in Fig. 1. With increase in the C_{inh} of *PPE* at 25 °C, v at first decreases and then stabilizes, whereas the change law of η is the reverse of that for v. At higher temperatures (35, 45, 55 °C), the decrease of v and the increase of η is continuous with increase of the tested C_{inh}. For the same C_{inh}, an increase of the temperature of the corrosion medium leads to a great increase in v and a decrease in η. These changes

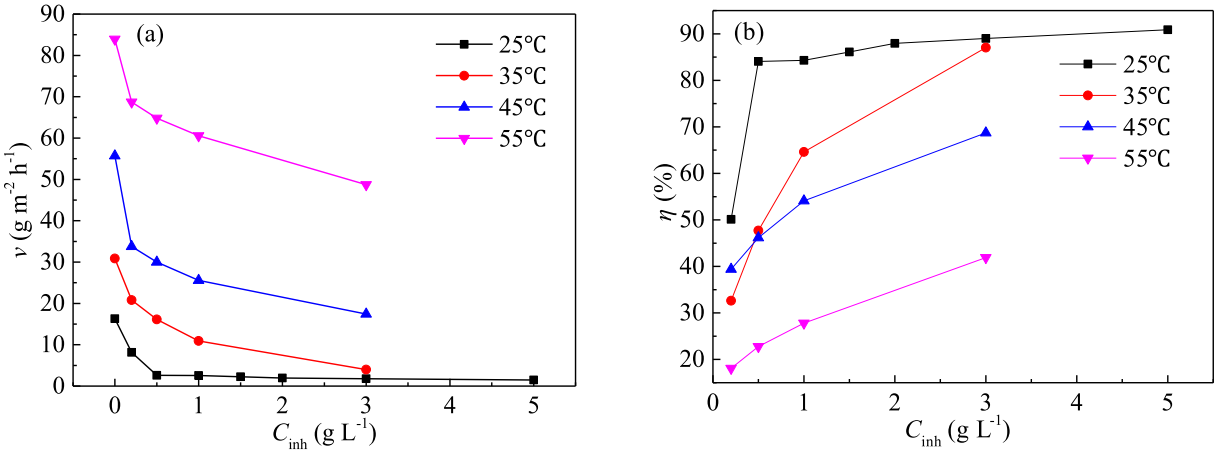

Fig. 1 Effect of C_{inh} and medium temperature on (a) v and (b) η in 1.0 mol/L H_3PO_4.

may reflect the following two phenomena. The adsorption capacity of the *PPE* molecules increases with C_{inh}. However, when the adsorption becomes saturated (e.g., at 25 °C and with 1.0 g/L *PPE*), the adsorption capacity would basically remain the same, thus v and η would be almost unchanged for higher C_{inh} (El-Etre and Abdallah, 2000; Mourya et al, 2014; Souza and Spinelli, 2009). Increasing the temperature of H_3PO_4 solution, the amount of hydrogen evolution on mild steel will thus increase. The evolution of hydrogen not only slows down the adsorption of the extract molecules on the metal surface, but also leads to desorption of the adsorbed molecules (El-Etre and Abdallah, 2000; Mourya et al, 2014; Souza and Spinelli, 2009). Thus, it is difficult to form a stable *PPE* adsorption film, which, in turn, causes an increase of v and a decrease of η. It can be inferred that the corrosion rate of mild steel and the inhibition efficiency of *PPE* are closely related to the temperature of the corrosion medium and the concentration of the extract inhibitor, which will determine the coverage of *PPE* on the surface of mild steel.

3.2. OCP curves

Measurement of the change in the OCP value with corrosion time is beneficial for understanding the adsorption and desorption equilibrium of extract molecules on the metal surface. The variation of OCP of mild steel in 1.0 mol/L H_3PO_4 solution at various C_{inh} is presented in Fig. 2. No matter whether *PPE* was added or not, the OCP tends to be stable within 1 h. The stable OCP with the addition of *PPE* is slightly more negative than that without inhibitor, and the difference is less than 10 mV. This indicates that the corrosion mechanism of mild steel in 1.0 mol/L H_3PO_4 solution was not appreciably altered and that *PPE* acts as a mixed type inhibitor (Ferreira et al., 2004; Gao et al., 2014). The corrosion inhibitor can be considered as an anode-type or a cathode-type inhibitor only when the change of corrosion potential was more than 85 mV (Satapathy et al., 2009).

3.3. PDP curves

The PDP curves for mild steel in 1.0 mol/L H_3PO_4 solution without and with various concentrations of *PPE* are presented in Fig. 3. The corresponding PDP parameters are listed in

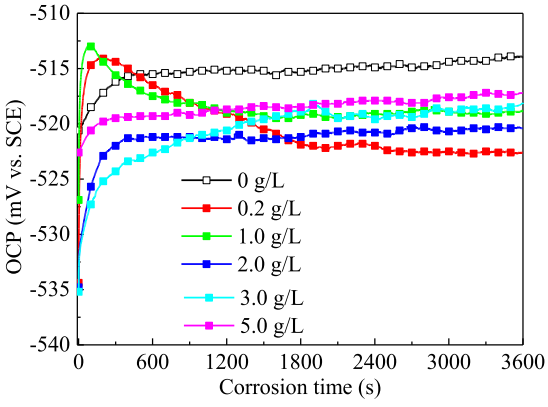

Fig. 2 Effect of *PPE* concentration on the OCP value of mild steel in 1.0 mol/L H_3PO_4.

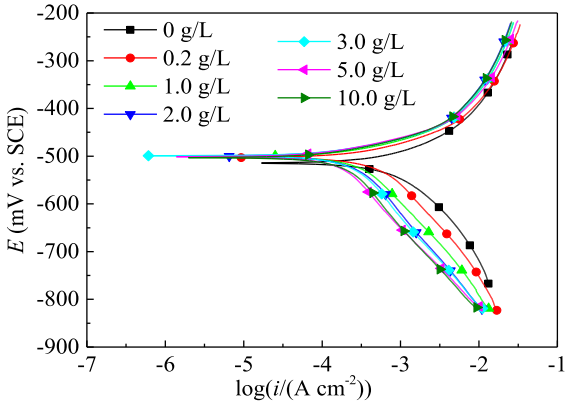

Fig. 3 Effect of the *PPE* concentration on the PDP curves for mild steel in 1.0 mol/L H_3PO_4.

Table 1. η of the *PPE* inhibitor based on PDP measurement was calculated by the expression

$$\eta(\%) = \frac{i^0_{corr} - i^{inh}_{corr}}{i^0_{corr}} \times 100\% \quad (3)$$

where i^0_{corr} and i^{inh}_{corr} are the corrosion current density of mild steel without and with *PPE*, respectively.

Compared with the blank case without *PPE* inhibitor, the addition of *PPE* in 1.0 mol/L H_3PO_4 solution reduces both the anode and cathode polarization current for mild steel; and the reduction range of the cathodic polarization current is slightly more obvious. This may be due to the adsorption of *PPE* molecules on the surface of mild steel. The corrosion potential (E_{corr}) of mild steel is only slightly changed in the presence of *PPE*, further indicating *PPE* functions as a mixed inhibitor (Solomon and Umoren, 2015; Talkhan et al., 2019). In addition, the anodic polarization curves are basically parallel to each other before and after addition of *PPE*, implying there is little difference in anodic Tafel slope (b_a) (Table 1) (Bahlakeh et al., 2019). Moreover, the cathodic curves generally are also parallel to each other and the differences of cathodic Tafel slope (b_c) are also very small. This suggests that the corrosion mechanism for mild steel in 1.0 mol/L H_3PO_4 solution is not changed by the presence of the *PPE* inhibitor, with oxidative dissolution of iron for the anode reaction and hydrogen evolution for the cathode reaction (Dehghani et al., 2019; Singh and Quraishi, 2016). Moreover, no matter whether *PPE* inhibitor was added or not, the corrosion system is controlled by the activated polarization control. All these phenomena indicate that the corrosion inhibition by *PPE* on mild steel can be attributed to the "geometric coverage" effect (Hamdani et al., 2015; Khaled, 2003). The adsorption film separates the mild steel surface from phosphoric acid solution, thus the electrode reactions cannot be carried out on the covered metal surface. However, the electrode reactions on the uncovered surface proceed according to the original process.

In acid solution, the organic matters in *PPE* will be protonated with hydrogen ions to form onium ions which are positively charged. Heteroatoms with lone-pair electrons (such as N, O, P, etc.) in organic compound will react with hydrogen ions to form coordination bonds. The covalent bond value of these elements is increased by one to become the corresponding cation, i.e. onium ions. The protonated positive ions

Table 1 Effect of the *PPE* concentration on the PDP parameters for mild steel in 1.0 mol/L H_3PO_4.

C_{inh} (g L^{-1})	E_{corr} (mV vs. SCE)	b_c (mV dec^{-1})	b_a (mV dec^{-1})	$i_{corr}\times10^{-4}$ (A cm^{-2})	η(%)	θ
0	−514	−156	139	11.1	–	–
0.2	−503	−180	131	7.68	30.8	0.308
1.0	−501	−169	133	5.12	53.9	0.539
2.0	−499	−200	142	4.58	58.7	0.587
3.0	−499	−203	141	4.37	60.6	0.606
5.0	−501	−194	120	3.23	70.9	0.709
10.0	−503	−208	128	3.22	71.0	0.710

will then undergo preferential adsorption on the cathodic active sites which are negatively charged. Therefore, the active area of the cathode is reduced obviously, which, in turn, slows down the cathode reaction rate. According to the working principle of the corrosive galvanic cell, the anode reaction rate will also be declined, reducing the anode current.

The coverage (θ) of *PPE* on the mild steel surface was calculated based on the η value

$$\theta = \eta/100 \tag{4}$$

As shown in Table 1, with the increase of the *PPE* concentration, i_{corr} at first decreases rapidly and then slowly, while η increases at first rapidly and then slowly. This indicates that the corrosion rate of mild steel and the corrosion protection efficiency of *PPE* directly depend on the "geometric coverage" of the *PPE* molecules on mild steel. The larger the "geometric coverage" by *PPE*, the greater the decrease in the corrosion rate for mild steel.

To evaluate the type of corrosion inhibition caused by the organic inhibitor, the anodic action coefficients (f_a) and the cathodic action coefficient (f_c) of the extract on mild steel under E_{corr} were calculated (Cao, 2008)

$$f_a = \frac{i_{corr}^{inh}}{i_{corr}^{0}\exp\left(\frac{E_{corr}^{inh}-E_{corr}^{0}}{\beta_a^0}\right)} \tag{5}$$

$$f_c = \frac{i_{corr}^{inh}}{i_{corr}^{0}\exp\left(-\frac{E_{corr}^{inh}-E_{corr}^{0}}{\beta_c^0}\right)} \tag{6}$$

where i_{corr}^0 and i_{corr}^{inh} are the corrosion current densities of mild steel in 1.0 mol/L H_3PO_4 solution without and with *PPE* inhibitor, respectively; E_{corr}^0 and E_{corr}^{inh} are the corrosion potentials without and with *PPE*, respectively; and β_a^0 and β_c^0 are the anodic and cathodic Tafel slope of mild steel in the absence of *PPE* inhibitor, respectively. The relationship between β and b can be expressed as $b = \beta\ln10 = 2.303\beta$.

Generally, if the value of f_a was smaller than one, the anodic reaction of the corrosion process of metal is inhibited. On the contrary, the anodic reaction is promoted. Similarly, the cathodic reaction is impeded when f_c was less than one. For the same corrosion system, the smaller f_a and f_c are, the stronger is the inhibition effect on the corresponding electrode reaction. The corrosion inhibitor can be regarded as a mixed inhibition type when $f_a \approx f_c$. And it can be judged as an anodic inhibition type for $f_a \gg f_c$ and a cathodic inhibitor type for $f_c \gg f_a$ (Cao, 2008).

The f_a and f_c values for *PPE* on mild steel in 1.0 H_3PO_4 solution are listed in Table 2. At all tested concentration of *PPE* inhibitor, the f_a and f_c values are smaller than one. For the same *PPE* concentration, the difference between f_a and f_c is very slightly and the ratio of f_a/f_c is highly close to one. It suggests that *PPE* has almost a similar inhibition effect on the anodic and cathodic reactions of mild steel. With the increase of *PPE* concentration, both f_a and f_c decrease, indicating an enhancement of the inhibition effect of the *PPE* inhibitor on mild steel. An analysis of the action coefficients confirms the above interpretation of the PDP curves.

3.4. EIS diagrams

The effect of the *PPE* concentration on the EIS diagrams for mild steel in 1.0 mol/L H_3PO_4 solution is presented in Fig. 4. As shown in Fig. 4(a), in the absence and presence of the *PPE* inhibitor, the Nyquist diagram for mild steel consists of a flattened capacitive loop at high frequency and an inductive loop at low frequency. The capacitive loop at high frequency corresponds to the electrical double layer capacitance and the charge transfer resistance at the steel/solution interface. The flattening of the capacitive loop is due to the dispersion effect associated with the roughness and heterogeneity of the electrode surface (Hamdani et al., 2015; Shih and Mansfeld, 1989). The inductive loop at low frequency may be related to the local corrosion of mild steel which probably caused by desorption of the *PPE* species from local sites of mild steel (Cao

Table 2 Effect of *PPE* concentration on the action coefficient for mild steel in 1.0 mol/L H_3PO_4 (at 25 °C).

Action coefficient	*PPE* concentration (g/L)					
	0.2	1.0	2.0	3.0	5.0	10.0
f_a	0.577	0.372	0.322	0.307	0.235	0.242
f_c	0.588	0.381	0.331	0.315	0.240	0.246
f_a/f_c	0.980	0.977	0.973	0.973	0.977	0.980

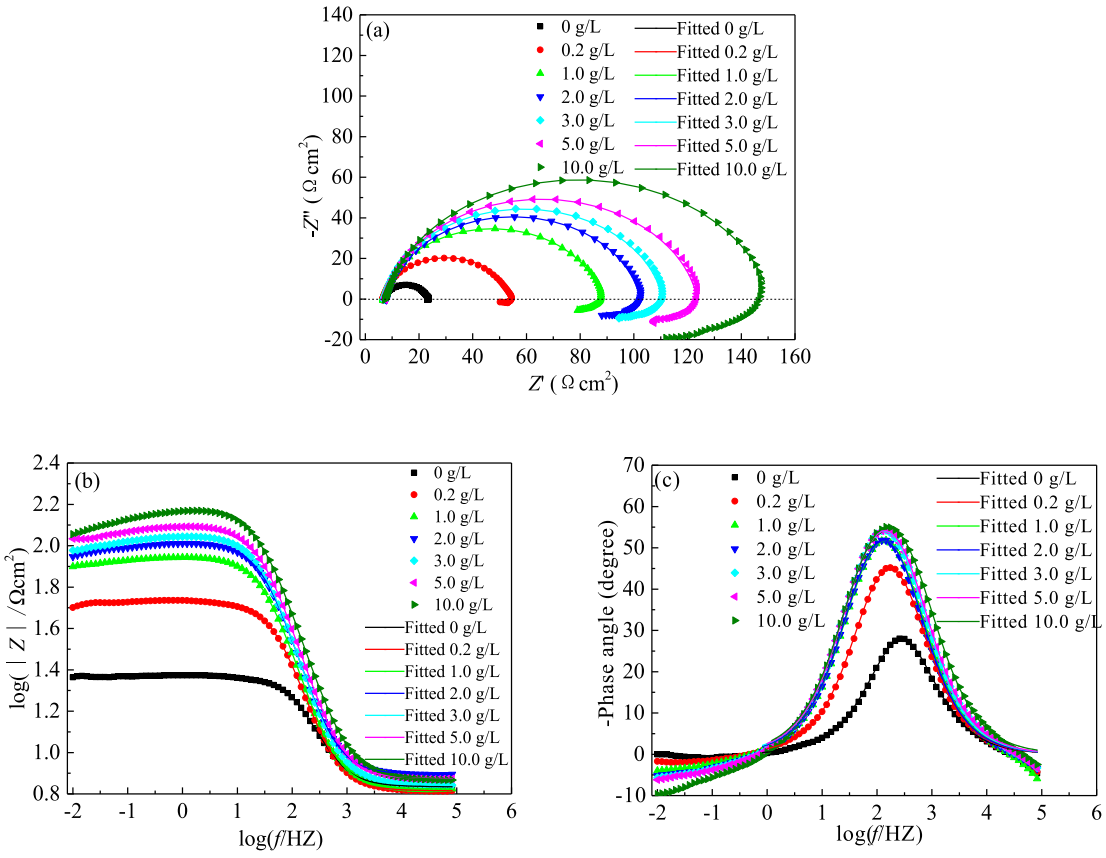

Fig. 4 Effect of *PPE* concentration on (a) Nyquist and (b), (c) Bode diagrams for mild steel in 1.0 mol/L H_3PO_4.

and Zhang, 2002; Pal et al., 2019; Shih and Mansfeld, 1989). However, the inductive loop increases with *PPE* concentration, which can be attributed to the re-adsorption of these charged species on local dissolution area of the mild steel surface. Therefore, the inductive loop can be used to explain desorption and re-adsorption of the extract molecules on the steel surface (Pal et al., 2019). The shape of the Nyquist diagram is not influenced by the *PPE* concentration, also suggesting that the corrosion behaviour for mild steel in H_3PO_4 is unchanged (Reis, et al., 2006; Solmaz, 2010). This is consistent with both the PDP and OCP results.

Furthermore, with the increase of the *PPE* concentration, the radius of the capacitive loop increases, indicating an increase in the charge transfer resistance of the corrosion reaction on mild steel. This may be attributed to an enhancement in the amount of extract adsorbed. Therefore, the coverage and density of the adsorbed film also increase, resulting in an improvement in the corrosion resistance of mild steel (Reis, et al., 2006; Solmaz, 2010).

As shown in Fig. 4b and c, the shape of the Bode diagram is almost unchanged for the addition of the *PPE* inhibitor. The width of the peak of the negative phase angle is narrow, suggesting that there is only one relaxation time constant for the capacitive loop at high frequency.

Fig. 5 shows the equivalent circuit used to fit the EIS diagrams in Fig. 4 (Cao, 2008; Pal et al., 2019). R_s is the solution resistance. R_L is the induction resistance and L is the inductance, which were invited to character the inductive loop in low frequency region. R_{ct} is the charge transfer resistance

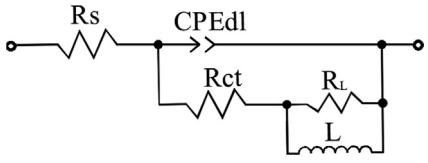

Fig. 5 Equivalent circuit used to fit the EIS diagrams in Fig. 4.

and CPE_{dl} is a constant phase angle element, which represents the electrical double layer capacitance of the steel/solution interface. The CPE is often used to describe the distortion capacitance in an actual electrochemical system (Cao and Zhang, 2002)

$$Z_{CPE} = \frac{1}{Y_0(j\omega)^n} \tag{7}$$

where Y_0 is an auxiliary parameter related to the value of the capacitance, ω is the angular frequency, j is the imaginary root, n is the distortion degree of the capacitance and ranges from 0 to 1. The smaller n is, the greater is the distortion of the capacitance and the surface roughness and non-uniformity of the capacitance. In contrast, the density and uniformity of the actual capacitance improves for a large value of n (Hamdani et al., 2015; Ma et al., 2000). The C_{dl} can be calculated by the following formula (Cao, 2008; Mobin et al., 2019; Qiang et al., 2018)

$$C_{dl} = Y_0 \cdot (\omega_{max})^{n-1} \tag{8}$$

where ω_{max} is the characteristic angular frequency and calculated by $2\pi f_{max}$. f_{max} corresponds to the characteristic frequency where the imaginary part of the high frequency capacitive loop in Nyquist diagram or the negative phase angle in Bode diagram is maximal.

In Nyquist diagrams, polarization resistance (R_p) is the real part of impedance when the tested frequency tends to the minimum value. Clearly, R_p is smaller than R_{ct} when inductive loop was present. η of *PPE* for mild steel was calculated based on R_{ct} (Cao, 2008; Pal et al., 2019)

$$\eta(\%) = \frac{R_{ct}^{inh} - R_{ct}^{0}}{R_{ct}^{inh}} \times 100\% \quad (9)$$

where R_{ct}^{0} and R_{ct}^{inh} are the charge transfer resistance of mild steel without and with inhibitor, respectively.

The corresponding fitted results for the EIS diagrams are presented in Table 3. The low value of R_s in 1.0 mol/L H_3PO_4 solution indicates the negligible impact of solution resistance on high frequency capacitive loop. In the presence of *PPE* inhibitor, the indexes corresponding to high frequency capacitive loop which indicate the enhancement of corrosion resistance of mild steel become better. That is, R_{ct}, n_{-dl}, η and θ increase, and Y_{0-dl}, C_{dl} and f_{max} decrease. And the improvement of these indexes can be attributed to the adsorption of *PPE* molecules on mild steel. Moreover, with the increase in concentration of *PPE* inhibitor, the corresponding indexes continuously improve.

Generally, R_{ct} may be used to characterize the degree of charge transfer difficulty between metal phase and solution phase due to the electrochemical reactions. When *PPE* molecules were adsorbed on the surface of mild steel, an adsorption film will cover on mild steel surface. The relative active area of mild steel decreases, and so is the active dissolution of mild steel. On one hand, the number of the migrated electrons decreases, leading to a reduction of i_{corr}. On the other hand, the adsorption film leads to an enhancement of the resistance of electron migration, i.e. an increase in R_{ct}. Therefore, the increase of R_{ct} with concentration of *PPE* can be attributed to the increase of coverage of *PPE* molecules on the electrode surface. To confirm the correlation between R_{ct} and the covered surface area, the relative electroactive area (REA) was calculated (Caio et al., 2019; Hamdani et al., 2015)

$$\text{REA} = 1 - \theta \quad (10)$$

The relationship between REA (date from PDP result) and R_{ct} is presented in Fig. 6 and exhibits a good linearity. Thus η and θ increase with the increase of concentration of *PPE* inhibitor.

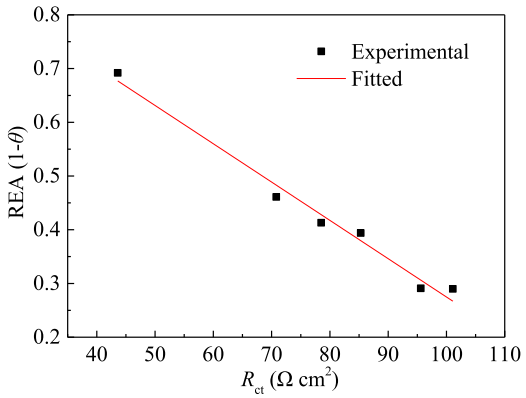

Fig. 6 Relationship between REA (data from PDP) and R_{ct}.

C_{dl} may be correlated to the electrode reactions and surface adsorption (Cao, 2008). During the electrode reactions, the excess charge between the solution phase and the metal phase of the electric double layer will generate. With the increase of coverage of *PPE* molecules on mild steel, the active dissolution of mild steel reduces, resulting in the decrease of the excess charge in electric double layer. C_{dl} is declined, too. Moreover, the surface adsorption also leads to the formation of electric double layer. The adsorption of *PPE* molecules on mild steel not only replaces the water molecules of which the dielectric constant is higher, but also increases the plate spacing of the electrical double layer capacitance and reduces the active surface area of mild steel in H_3PO_4 solution (Outirite et al., 2010). According to the Helmholtz model (Hu et al., 2017, Qiang et al., 2018)

$$C = \frac{\varepsilon^0 \varepsilon S}{d} \quad (11)$$

where C is the capacitance of plate capacitor, S is the surface area, ε^0 is the vacuum dielectric constant, ε is the local dielectric constant, d is the distance between the two plates. It further suggests that the decrease of C_{dl} is due to the adsorption of *PPE* molecules on mild steel. As mentioned above, C_{dl} is closely related to the coverage of *PPE* molecules on the surface of mild steel. The relationship between the REA (data from PDP) and C_{dl} is given in Fig. 7 and it also shows a good linearity, similar to that of R_{ct} in Fig. 6. It can be proved that the inhibition mechanism of *PPE* is "geometric coverage" effect. This is consistent with the PDP results.

As shown in Table 3, n_{-dl}, which characterizes the dispersion effect of the capacitance of the electrical double layer at the mild steel-solution interface, is very close to one. This cor-

Table 3 Fitting parameters for EIS data of mild steel in H_3PO_4 with various concentrations of *PPE*.

C_{inh} (g L^{-1})	R_s (Ω cm^2)	Y_{0-dl} ($\mu\Omega^{-1}cm^{-2}$ s^n)	n_{-dl}	R_{ct} (Ω cm^2)	R_L (Ω cm^2)	L (Ω cm^2)	f_{max} (Hz)	C_{dl} (μF cm^{-2})	η (%)	θ
0	6.8	184.0	0.861	18.6	–	–	146.5	71.2	–	–
0.2	6.5	112.2	0.901	43.6	3.9	26.8	56.23	62.8	57.3	0.573
1.0	6.7	102.8	0.899	70.8	10.4	44.6	31.62	60.2	73.7	0.737
2.0	7.8	87.9	0.903	78.5	16.0	65.0	31.62	52.6	76.3	0.763
3.0	7.0	87.8	0.900	85.3	18.5	66.7	31.62	51.7	78.2	0.782
5.0	7.5	80.8	0.894	95.6	20.8	70.5	31.62	46.1	80.5	0.805
10.0	7.4	72.1	0.879	101.1	38.5	140.2	26.10	38.9	81.6	0.816

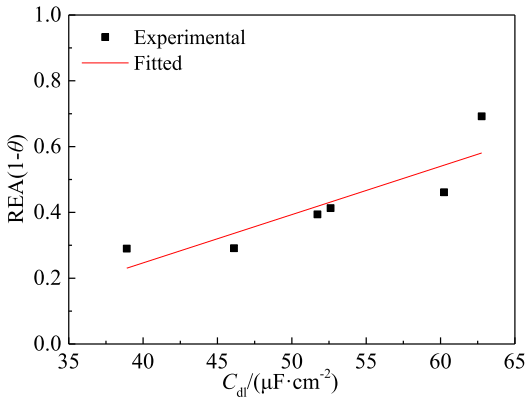

Fig. 7 Relationship between REA (data from PDP) and C_{dl}.

responds well to a relatively regular capacitive loop as shown in Fig. 4a. In the presence of *PPE* inhibitor, $n_{\text{-dl}}$ increases but the overall change is small. It can be considered that the surface roughness, density and uniformity of mild steel in 1.0 mol/L H_3PO_4 solution are good.

R_L and L were used to denote the inductive loop in low frequency region. R_L is related to the resistance of the local repair layer due to the re-adsorption of the charged species, and L can be attributed to the variation of current flux for these charged particles (Pal et al., 2019). In the absence of *PPE* inhibitor, R_L and L were not fitted due to the very small low frequency inductive loop. That is, the local corrosion of mild steel in low frequency region could not be repaired because there was no corrosion inhibitor. In the presence of *PPE* inhibitor, both R_L and L improve with an increase in concentration of *PPE*. It suggests that desorption and re-adsorption of the extract molecules on surface of mild steel are enhanced and the active surface is repaired more effectively (Cao, 2008; Pal et al., 2019). Therefore, the corrosion of mild steel is impeded.

3.5. Corrosion morphology

The effects of the *PPE* on the corrosion morphology of mild steel sample immersed in 1.0 mol/L H_3PO_4 solution for 1 h are shown in Fig. 8. In the absence of the *PPE* inhibitor, the surface of mild steel is rough, and numerous corrosion products are evident. In the presence of 1.0 g/L *PPE*, the surface is relatively flat, with a large number of dense and needle-like corrosion products (in Fig. 8c). At higher magnification, the edge and surface of the needle-like plates are covered with denser and finer needle-like products (in Fig. 8d). When the *PPE* was increased to 5.0 g/L, the density and surface smoothness of the mild steel sample is further improved (in Fig. 8e and f). The above phenomena indicate that the presence of *PPE* in 1.0 mol/L H_3PO_4 solution is beneficial to the formation of a continual corrosion-resistant film on mild steel. Also, *PPE* may be adsorbed on the mild steel surface. As a result, corrosion of mild steel is effectively inhibited.

3.6. Effectiveness of corrosion protection by PPE

To evaluate the effectiveness of corrosion protection by *PPE*, the EIS diagrams for mild steel in 1.0 mol/L H_3PO_4 solution containing 5.0 g/L *PPE* at room temperature were acquired, as shown in Fig. 9. For corrosion times in the range from 0.5 to 47 h, the shape of the EIS diagrams for mild steel remained unchanged. There is a high frequency capacitive loop correlated to the electrical double layer capacitance and the charge transfer resistance at the steel/solution interface and a low frequency inductive loop attributed to desorption and re-adsorption of *PPE* molecules on local dissolution sites of mild steel. However, for corrosion times up to 224 h, the shape of the EIS diagrams is changed. The peak width of the negative phase angle on the Bode diagrams is also increased. They contain a high-frequency capacitive loop, a middle-frequency capacitive loop and

a low-frequency inductive loop. Therefore, the corrosion behaviour for mild steel is altered for prolongation of immersion time. For the longer corrosion times (up to 224 h), the corrosion reaction is not only controlled by the electrical double layer capacitance and the charge transfer resistance of the steel-solution interface, but also dependent on the film capacitance and film resistance on the surface of mild steel. The appearance of the film capacitance and the film resistance may be contributed to the over adsorption of *PPE* molecules, a decrease of film density, etc. (Hamdani et al., 2015).

The EIS diagrams corresponding to corrosion for 0.5–47 h and 224–315 h were analysed and fitted by the equivalent circuits illustrated in Figs. 5 and 10, respectively (Mobin et al., 2019; Pal et al., 2019). CPE_c and R_c were applied to characterize the capacitance and resistance of the protection film. It can be seen that the fitting data coincides well with the experimental data. Thus the equivalent circuits are realistic and feasible.

The fitted results are presented in Table 4. For corrosion time of 224–315 h, the contribution of film resistance to the corrosion inhibition efficiency of *PPE* should be considered. And the sum of R_c and R_{ct}, denoted as R_{tot}, was used to calculated η of *PPE* for mild steel (Cao, 2008)

$$\eta(\%) = \frac{R_{tot}^{inh} - R_{ct}^{0}}{R_{tot}^{inh}} \times 100\% \quad (13)$$

where R_{ct}^{0} is the charge transfer resistance of mild steel in 1.0 mol/L H_3PO_4 solution without inhibitor after corrosion for 1 h (i.e. 18.6 Ω·cm^2), and R_{tot}^{inh} is the sum of R_c and R_{ct} of mild steel in 1.0 mol/L H_3PO_4 solution with 5.0 g/L *PPE* for longer corrosion time.

As shown in Table 4, for immersion time ranged from 0.5 h to 47 h, the $n_{\text{-dl}}$ value is high and almost is unchanged, suggesting a good density and compactness of mild steel surface. However, $n_{\text{-dl}}$ decreases for longer corrosion time of 224 h and 315 h, which may be due to the over adsorption of *PPE* on mild steel, resulting in a coarse surface (Hamdani et al., 2015). Moreover, with the increase of immersion time, $Y_{0\text{-dl}}$ and C_{dl} at first decline and then increase; and R_{ct} (or R_{tot}) improves firstly followed by a decrease. The inflection point occurs at 23 h, and so is the inhibition efficiency and coverage of *PPE* inhibitor.

As far as the inductive loop was concerned, R_L and L at first increase and then drop. The turning point is at 5 h, which can also be confirmed by the longest inductive loop in low frequency region when the immersion time was 5 h. Because the inductive loop reflects the capacity of desorption and re-adsorption of *PPE* molecules on mild steel surface. For longer immersion time, the weakening of desorption and re-

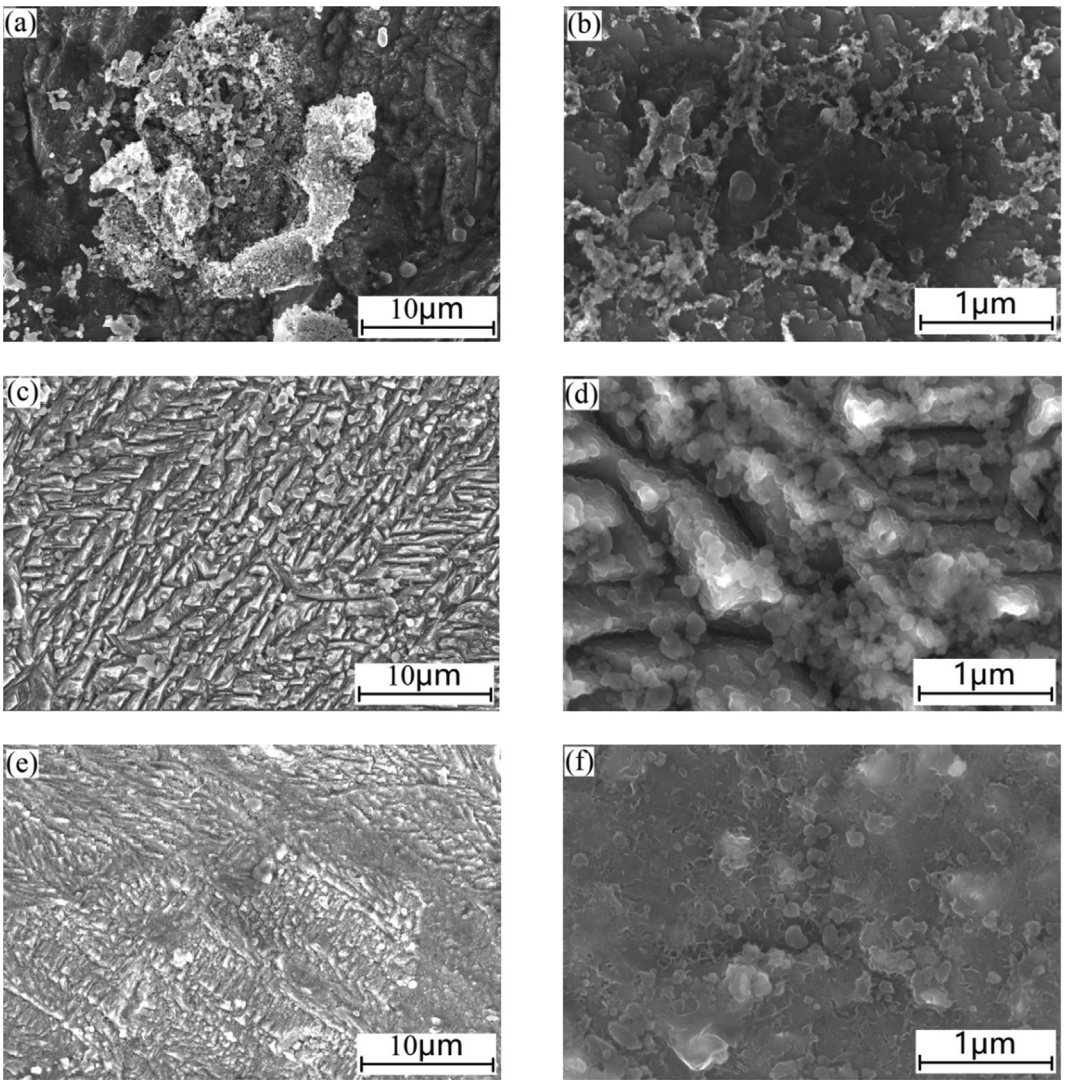

Fig. 8 Effect of *PPE* on the corrosion morphology of mild steel in 1.0 mol/L H_3PO_4 medium: (a), (b) without *PPE*; (c), (d) with 1.0 g/L *PPE*; (e), (f) with 5.0 g/L *PPE*.

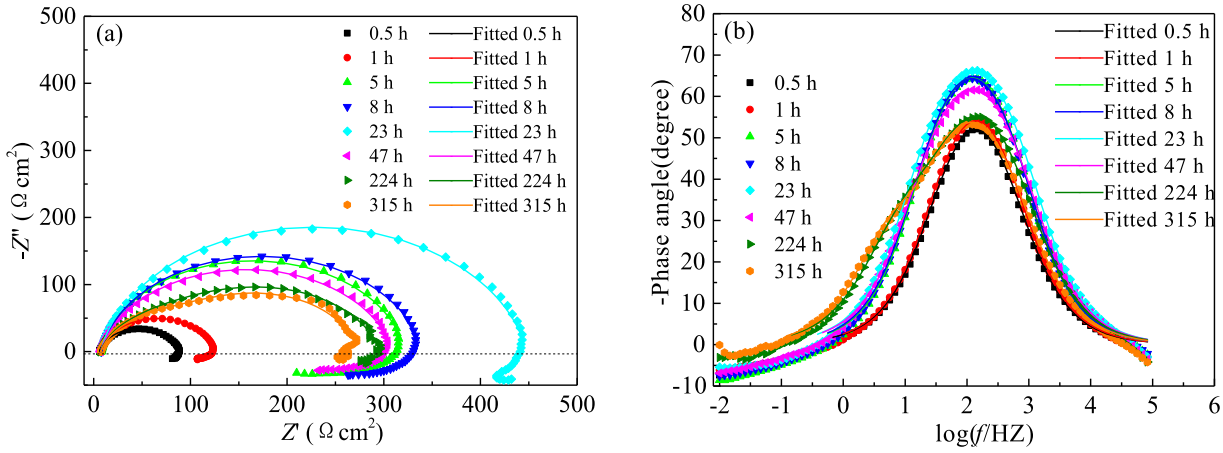

Fig. 9 EIS diagrams for mild steel immersed in 1.0 mol/L H_3PO_4 solution with 5.0 g/L *PPE* for different times: (a) Nyquist diagrams; (b) Negative phase angle for Bode diagrams.

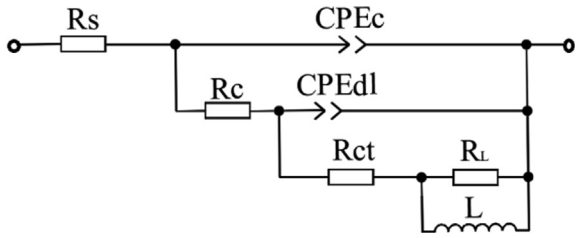

Fig. 10 Equivalent circuit used to fit the EIS diagrams under longer corrosion times (224-315 h).

adsorption ability at low frequency may be related to the more complicated surface and the untimely supplement of *PPE* molecules to the local dissolved surface.

The density and compactness of the adsorption film and the capacity of desorption and re-adsorption of *PPE* molecules becomes poor for longer immersion time. However, the η value of *PPE* inhibitor still is up to 91.9% after corrosion for 315 h, much higher than the value of 80.5% for immersion only 1 h. It can be concluded that *PPE* confers a long-term and effective inhibition for mild steel in 1.0 mol/L H_3PO_4 solution.

Table 5 shows comparison of *PPE* results with other plant extract as inhibitors for metal in acid solution. Clearly, most plant extract followed the Langmuir adsorption isotherm and functioned as the mixed inhibitor. In present work, the adsorption isotherm is influenced by the medium temperature and *PPE* simultaneously obeys the Langmuir, El-Awady and Temkin isotherms at 35, 45 and 55 °C. The maximum efficiency of different plant extract also exhibits a certain difference. On the whole, the concentration of plant extract in 1.0 mol/L HCl solution is relatively low, but most of them display good corrosion inhibition efficiency. This may be related to the synergistic inhibition effect of the mixed inhibitor of organic compound and halide ions due to the bridging principle (ElKacimi et al., 2020; Li and Deng, 2020; Qian et al., 2013). On the contrary, the extract inhibitor concentration in H_2SO_4 and H_3PO_4 media is relatively high. In H_3PO_4 solution, *PPE* has obvious advantage as corrosion inhibitor with inhibition efficiency of 95%. It further suggests that *PPE* has great potential as a green, long lasting, efficient and renewable corrosion inhibitor for mild steel in phosphoric acid medium.

3.7. Adsorption isotherm

Electrochemical analysis indicated that the inhibition mechanism of *PPE* on mild steel in 1.0 mol/L H_3PO_4 solution proceeded through a "geometric coverage" effect. The corrosion of mild steel was closely related to its REA as depicted in Figs. 6 and 7. A protective film was formed by the adsorption of the *PPE* inhibitor on the surface of mild steel. Based on the result of mass loss test, various adsorption isotherms were examined in an attempt to clarify the adsorption behaviour of *PPE*. The results show that the adsorption can be explained by the Langmuir, the El-Awady and the Temkin isotherms (Faustin et al., 2015; Ituen et al., 2017; Jyothi and Ravichandran, 2014). The fitted results are presented in Fig. 11, and the corresponding parameters are given in Tables 6–8.

The respective adsorption isotherms are as follows:

Langmuir isotherm:

Table 4 EIS parameters for mild steel in 1.0 mol/L H_3PO_4 with 5.0 g/L *PPE* for different immersion times (t).

t(h)	R_s(Ωcm^2)	$Y_{0\text{-}c}$($\mu\Omega^{-1}$cm^{-2}s^{n})	$n_{\text{-c}}$	R_c(Ωcm^2)	$Y_{0\text{-}dl}$($\mu\Omega^{-1}$cm^{-2}s^{n})	$n_{\text{-dl}}$	R_{ct}(Ωcm^2)	R_L(Ωcm^2)	L(Ωcm^2)	$f_{max(Hz)}$	C_{dl}(μFcm^{-2})	η(%)	θ
0.5	8.5	–			88.6	0.888	82.1	18.7	59.3	31.62	49.0	77.3	0.773
1	7.5				80.8	0.894	95.6	20.8	70.5	31.62	46.1	80.5	0.805
5	7.7				49.2	0.909	214.5	92.0	298.0	14.68	32.6	91.3	0.913
8	8.0				48.3	0.914	250.3	76.2	282.6	14.68	31.3	92.6	0.926
23	7.3				47.9	0.891	369.8	71.3	195.4	12.12	29.9	95.0	0.950
47	7.0				69.2	0.868	328.8	69.0	190.4	14.68	38.1	94.3	0.943
224	7.0	117.3		0.856	147.7	350.9	0.796	111.4	32.7	181.5	2.61	198.3	92.8	0.928
315	7.3	121.6		0.845	129.0	378.8	0.778	99.6	19.7	40.9	2.61	203.6	91.9	0.919

R_{tot} at 224 h and 315 is 259.1 and 228.6 Ω·cm^2, respectively.

Table 5 Comparison of *PPE* results with other plant extract inhibitors in acid solutions.

Extract inhibitor	Metal	Corrosion solution	Content (g L^{-1})	Maximum efficiency (%)	Inhibition type	Adsorption isotherm	Reference
Ginkgo leaf	X70 steel	1 mol/L HCl	0.2	90	Mixed	Langmuir	Qiang et al., 2018
Musa paradisica peel	Mild steel	1 mol/L HCl	0.3	90	Anodic	–	Ji, et al., 2015
Retama monosperma (L.) Boiss.	Mild steel	1 mol/L HCl	0.4	94	Mixed	Langmuir	Hamdani et al., 2015
Glycyrrhiza glabra	Mild steel	1 mol/L HCl	0.8	88	Mixed	Langmuir	Alibakhshi et al., 2018
Borage flower	Mild steel	1 mol/L HCl	0.8	91	Mixed	Langmuir	Dehghani et al., 2020
Peganum harmala seed	Mild steel	1 mol/L HCl	0.8	94	Mixed	Freundlich	Bahlakeh et al., 2019
Pineapple stem	Carbon steel	1 mol/L HCl	1.0	97	Mixed	Langmuir	Mobin et al., 2019
Ircinia strobilina	Mild steel	1 mol/L HCl	2.0	84	Mixed	Langmuir	Caio et al., 2019
Tagetes erecta	Mild steel	0.5 mol/L H_2SO_4	1.0	96	Mixed	Langmuir	Mourya et al., 2014
Litchi Chinensis peels	Mild steel	0.5 mol/L H_2SO_4	3.0	98	Mixed	Langmuir	Singh et al., 2019
Garlic (Allium Sativum)	Copper	8 mol/L H_3PO_4	1.8	78	–	–	Taha et al., 2020
Artemisia herba-alba	Stainless steel	1 mol/L H_3PO_4	1.0	88	Mixed	Langmuir	Boudalia et al., 2019
Apricot juice	Mild steel	1 mol/ LH_3PO_4	40.0	75	–	Langmuir	Yaro et al., 2013
Guar gum	Carbon steel	2 mol/L H_3PO_4	1.0	96	Mixed	Temkin	Messali et al., 2017
Crab waste protein	Carbon steel	2 mol/L H_3PO_4	4.97	94	Mixed	Langmuir	Ismail et al., 2020
Pomelo peel	Mild steel	1 mol/L H_3PO_4	5.0	95	Mixed	Langmuir, El-Awady, and Temkin	Present work

$$\frac{C_{\text{inh}}}{\theta} = \frac{1}{K_{\text{ads}}} + C_{\text{inh}} \tag{14}$$

El-Awady isotherm:

$$\ln\frac{\theta}{1-\theta} = \ln K' + y\ln C_{\text{inh}} \tag{15}$$

Temkin isotherm:

$$\theta = -\frac{1}{2\alpha}\ln C_{\text{inh}} - \frac{1}{2\alpha}\ln b \tag{16}$$

where θ is the coverage of *PPE* on the surface of mild steel and was calculated as $\theta = \eta/100$, the η values being derived from the mass loss experiments; C_{inh} is the mass concentration of *PPE* (g/L); K_{ads} is the adsorption equilibrium constant (L/g); $1/y$ is the number of water molecules which are replaced by one inhibitor molecule. The relationship between K' and K_{ads} was converted using the expression $K_{\text{ads}} = K'^{(1/y)}$ (Deyab and Abd El-Rehim, 2012; Jyothi and Ravichandran, 2014); b is the Temkin isothermal constant; α is the transverse molecular interaction parameter used to predict whether there is an attractive or repulsive force in the adsorption layer (Faustin et al., 2015; Shukla and Ebenso, 2011). When α is negative, there is an intermolecular repulsion force in the adsorption film; otherwise, there is an intermolecular attractive force in the adsorption layer.

It should be pointed out that the Langmuir isotherm can be used to predict whether the adsorption film is a single molecular layer; the El-Awady isotherm can be used to examine the number of the water molecules that can be replaced by one inhibitor molecules on the metal surface; and the Temkin isotherm can be used to predict the interaction forces operating between molecules in the adsorption film (Caio et al., 2019; Deyab and Abd El-Rehim, 2012; Faustin et al., 2015; Jyothi and Ravichandran, 2014; Shukla and Ebenso 2011).

As shown in Fig. 11a, there is a good linear relationship between C_{inh}/θ and C_{inh} at four experimental temperatures (25, 35, 45 and 55 °C), and the correlation coefficient (R^2) is very close to one. It suggests that the adsorption of *PPE* on the surface of mild steel conforms to the Langmuir isotherm and is monolayer adsorption.

The K_{ads} can be used to characterize the adsorption degree of inhibitor molecules from the solution to the metal surface. Generally, the higher the K_{ads} value is, the stronger is the adsorption capacity of organic molecules on the metal surface, and the better is the inhibition effect (Caio et al., 2019; Hamdani et al., 2015; Hassannejad and Nouri, 2018; Mhiri et al., 2016; Nikpour et al., 2019; Sin et al., 2017; Wang et al., 2019). According to the intercept of the fitting line of the Langmuir isotherm, K_{ads} can be calculated, as shown in Table 5.

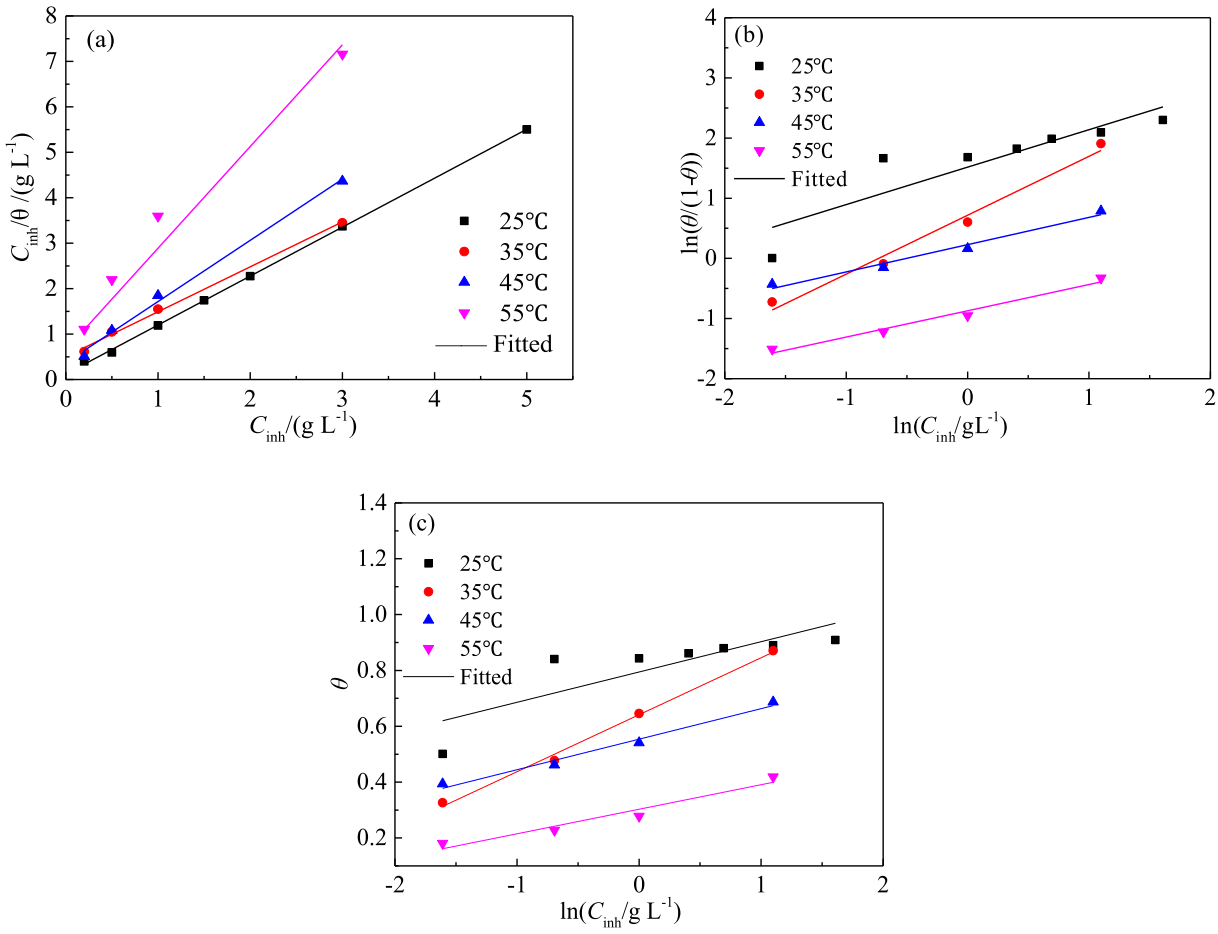

Fig. 11 Adsorption isotherms for *PPE* on mild steel surface (a) Langmuir; (b) El-Awady; (c) Temkin.

Table 6 Fitting results of the Langmuir isotherm for *PPE* on mild steel.

T (°C)	Correlation coefficient (R^2)	Intercept	Slope	K_{ads}(L g^{-1})	ΔG_{ads}(kJ mol^{-1})
25	1.000	0.122	1.07	8.2	−22.1
35	0.999	0.502	0.99	2.0	−19.2
45	0.998	0.369	1.35	2.7	−20.6
55	0.991	1.080	2.08	0.9	−18.3

Table 7 Fitting results of the El-Awady isotherm for *PPE* on mild steel.

T (°C)	R^2	Intercept	Slope	1/y	K_{ads}(L g^{-1})	ΔG_{ads}(kJ mol^{-1})
25	0.896	1.516	0.62	1.61	11.4	−22.9
35	0.992	0.717	0.98	1.02	2.1	−19.3
45	0.989	0.228	0.45	2.21	1.7	−19.4
55	0.989	−0.871	0.44	2.29	0.1	−12.3

As shown in Fig. 11a and Table 6, with an increase in the temperature of the corrosion medium, K_{ads} decreases, resulting in a decrease in the adsorption force of *PPE*. This reflects the fact that the hydrogen evolution reaction increases with the temperature of the corrosion medium, such that the mechanical stripping of the evolution of hydrogen atoms leads to desorption of the adsorbed extract and a decrease in the adsorption capacity and coverage of the extract. This is consistent with the changes of v_{corr} and η with the temperature of the corrosion medium. It further indicates that a high temperature

Table 8 Fitting results of the Temkin isotherm for *PPE* on mild steel.

T (°C)	R^2	Intercept	Slope	α
25	0.834	0.794	0.11	−4.607
35	0.998	0.641	0.20	−2.450
45	0.991	0.554	0.11	−4.574
55	0.974	0.303	0.09	−5.688

is not beneficial to the adsorption of *PPE* molecules (Bahlakeh et al., 2019; Hassannejad and Nouri, 2018). In addition, dispersion of the Langmuir fitting line increased at 55 °C, which may be related to a little change in the adsorption model (Alrefaee et al., 2020; Divya et al., 2019).

As shown in Fig. 11b and c, except at 25 °C, the adsorption of *PPE* on mild steel at 35, 45 and 55 °C not only obeys the Langmuir isotherm, but also follows the El-Awady and Temkin isotherms.

As shown in Table 7, the K_{ads} values obtained from the El-Awady isotherm are in good agreement with those obtained by the Langmuir isotherm. All values of $1/y$ obtained by the El-Awady fitting lines were greater than one. One extract molecule can replace multiple water molecules. That is, one extract molecule occupies multiple active points on the surface of mild steel (Jyothi and Ravichandran, 2014). The value of $1/y$ is distinct at different temperatures, which may be related to the different adsorption performance, such as physical, chemical and mixed adsorption (Divya et al., 2019).

As shown in Table 8, the negative values for α obtained from the Temkin isotherm indicate a repulsive force is operating in the adsorption layer (Deyab and Abd El-Rehim, 2013). The rejection strength decreases in the following order: 55 °C > 45 °C > 35 °C. This also corresponds to the change trend of the surface coverage with medium temperature.

3.8. Adsorption thermodynamics of PPE

To further explore the adsorption behaviour of *PPE* at the mild steel-solution interface, the *Gibbs free energy* (ΔG_{ads}) was calculated (Hamdani et al., 2015; Hu et al., 2016; Obi-Egbedi et al., 2015)

$$K_{ads} = \frac{1}{\rho_{solvent}} \exp\left(-\frac{\Delta G_{ads}}{RT}\right) \tag{17}$$

where R is the gas constant (8.314 J/(K mol)); T is the absolute temperature (K); and $\rho_{solvent}$ is the mass concentration of the solvent (g/L). Except the content of phosphoric acid and *PPE* inhibitor, $\rho_{solvent}$ in 1.0 mol/L H_3PO_4 solution is approximately 900 g/L. The calculated results for ΔG_{ads} are listed in Tables 6 and 7.

Generally, when ΔG_{ads} was higher than −20 kJ/mol, the adsorption can be regarded as physical adsorption; whereas it is chemical adsorption for ΔG_{ads} was smaller than −40 kJ/mol (Hamdani et al., 2015; Hu et al., 2016; Obi-Egbedi et al., 2015). Physical adsorption mainly results in the formation of an adsorbed layer due to the electrostatic attraction between the charged inhibitor molecules and the charged metal surface. In the case of chemical adsorption, a protection film is formed mainly through the charge transfer or the charge sharing between the inhibitor molecules and the metallic constituents on the metal surface (Deyab and Abd El-Rehim, 2013; Hu et al., 2016; Obi-Egbedi et al., 2015). As shown in Tables 6 and 7, the ΔG_{ads} values obtained by the Langmuir and the El-Awady adsorption isotherms are basically consistent. At all test temperatures, ΔG_{ads} is negative. The adsorption of *PPE* molecules on the surface of mild steel in 1.0 mol/L H_3PO_4 solution is spontaneous. In addition, at room temperature (25 °C), the adsorption model of *PPE* on mild steel is mixed adsorption with main pattern of physical adsorption. At higher temperatures, the adsorption model of *PPE* is physical adsorption, and the adsorption propensity and capacity decrease. It should be pointed out that in acidic media, organic matters in *PPE* would be protonated and thus were positively charged, resulting in the formation of charged molecules (Caio et al., 2019; Deyab and Abd El-Rehim, 2013; Hamdani et al., 2015).

3.9. Kinetic parameters for adsorption

The results for the adsorption thermodynamics indicate that the temperature of the corrosion medium is one of the most important parameters to affect the inhibition performance of *PPE*. In accord with the Arrhenius equation and the Transition State theory, the influence of *PPE* on the corrosion kinetics of mild steel in 1.0 mol/L H_3PO_4 solution was subsequently examined (Dkhireche et al., 2020). The Arrhenius equation and the Transition State theory equation were respectively expressed as

$$\ln v = \ln A - \frac{E_a}{RT} \tag{18}$$

$$\ln\left(\frac{v}{T}\right) = -\frac{\Delta H_a}{RT} + \frac{\Delta S_a}{R} + \ln\left(\frac{R}{Nh}\right) \tag{19}$$

where v is the corrosion rate of mild steel based on mass loss test; A is the pre-exponential factor; E_a is the activation energy for the reaction of mild steel; R is the gas constant; T is the absolute temperature; N is the Avogadro constant (6.02×10^{23}); h is the Plank constant (6.626×10^{-34} J/s); and ΔH_a and ΔS_a are the activation enthalpy and the activation entropy for the corrosion reaction of mild steel, respectively.

E_a is the minimum energy required to judge whether a reaction can occur. ΔH_a can be used to assess the endothermic or exothermic process of the metal dissolution; and the adsorption model of the physical adsorption, chemical adsorption or mixed adsorption of corrosion inhibitor will thus be judged. ΔS_a can be used to evaluate the order of the metal surface. And A reflects the number of active points in the heterogeneous reaction. These physical and chemical adsorption parameters are helpful aids in clarifying the inhibition behaviour of the extract.

According to the equations of the Arrhenius and Transition State theory, the experimental data based on the mass loss tests were analysed, as shown in Fig. 12. The fitting results for both adsorption kinetic equations were found to be linear. Based on the slopes and intercepts for the fitting lines, the parameters (E_a, ΔH_a and ΔS_a) for activation of the corrosion reaction were calculated, as shown in Table 9. In the absence of inhibitor, the value of E_a is about 43.9 kJ/mol, but it is up to 92.3 kJ/mol in the presence of 3.0 g/L *PPE*. E_a is enhanced obviously with increase in the *PPE* concentration. It indicates that the

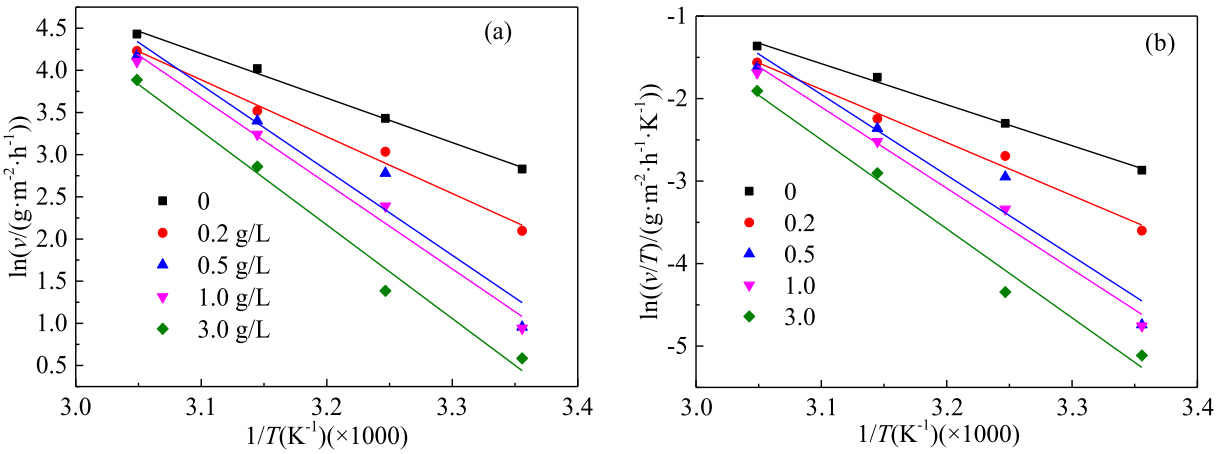

Fig. 12 Effect of the *PPE* concentration on the adsorption kinetics of the activation reaction for mild steel: (a) the Arrhenius line of ln (v) ~ $1/T$; (b) the Transition State theory line of ln(v/T) ~ $1/T$.

Table 9 Effect of the *PPE* concentration on kinetic parameters for activation reaction of mild steel.

C_{inh}(gL^{-1})	A	E_a(kJmol^{-1})	ΔH_a(kJmol^{-1})	ΔS_a(Jmol^{-1}K^{-1})
0	8.6×10^8	43.9	41.3	−82.6
0.2	5.8×10^{10}	56.0	53.4	−47.6
0.5	1.8×10^{15}	83.9	81.3	38.4
1.0	1.7×10^{15}	84.3	81.7	38.2
3.0	2.3×10^{16}	92.3	89.7	59.7

addition of the *PPE* inhibitor makes the corrosion reaction of mild steel more difficult due to the formation of the *PPE* adsorption film on the surface of mild steel.

Moreover, the variation of A with the *PPE* concentration is the same as that for E_a, and the enlargement range for the solution with 3.0 g/L *PPE* was nearly eight orders of magnitude greater compared to the results for the solution without inhibitor. That is, the disorder of the corrosion system is increased (Ech-chihbi et al., 2020). On one hand, the competitive adsorption between the water molecules and the protonated extract ions on the metal surface make the adsorption and desorption phenomenon become more frequent, and the disorder caused by this competitive adsorption is far greater than the ordering due to the *PPE* molecular adsorption (Ansari et al., 2014; Ech-chihbi et al., 2020; Khan et al., 2017). On the other hand, the rate determination step of the activated complex is a discrete separation step rather than an associated step, resulting in an increase in disorder for the transfer process from reactants to activated complexes (Ansari et al., 2014). Consequently, there is an increase in ΔS_a with *PPE* concentration as indicated in Table 9.

The change of the activation parameters (E_a and A) with *PPE* concentration indicates that the corrosion reaction for mild steel is not only related to the energy of the corrosion system, but also is correlated to the active points of the heterogeneous reactions and the degree of disorder of A and ΔS_a for the whole system (Ansari et al., 2014).

Fig. 13 shows the relationship between ΔH_a and E_a for the corrosion reaction of mild steel in 1.0 mol/L H_3PO_4 solution. ΔH_a and E_a exhibit a strict linearity with relationship of $\Delta H_a = E_a - 2.62$. The average difference is 2.62 kJ/mol,

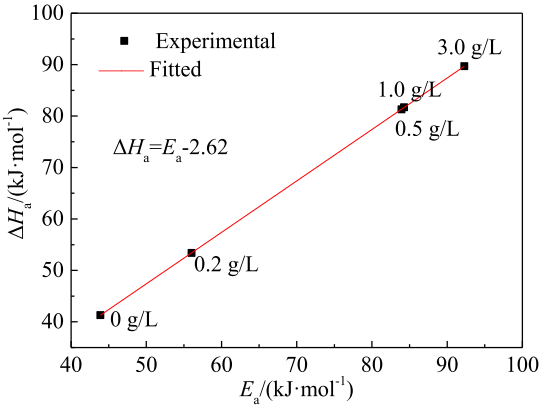

Fig. 13 Relationship between ΔH_a and E_a for the corrosion reaction of mild steel.

indicating a very close value of E_a to ΔH_a of which was obtained by the Transition State theory. It can be explained by thermodynamic equation of the mono-molecular reaction of ideal gas (Nathiya and Raj, 2017)

$$\Delta H_a = E_a - RT \tag{20}$$

The average temperature used to calculate ΔH_a and E_a in this study was 313 K. The average RT was 2.60 kJ/mol, very close to the fitting value of 2.62 kJ/mol. It thus suggests that the anodic reaction of mild steel in 1.0 mol/L H_3PO_4 solution is a mono-molecule reaction.

As shown in Table 9, the value of ΔH_a under all conditions is positive, indicating that the dissolution reaction of mild steel in 1.0 mol/L H_3PO_4 medium is an endothermic process. This is consistent with the clear increase of the corrosion rate of mild steel with temperature of the corrosion medium (Fig. 1). Moreover, ΔH_a increases with the addition of the *PPE* inhibitor. Due to the adsorption of *PPE* on the surface of mild steel, the dissolution reaction of mild steel needs to absorb more energy. The adsorption of *PPE* makes the corrosion process of mild steel more difficult. Generally, the absolute value of ΔH_a for physical adsorption is lower than 80 kJ/mol, while that of chemical adsorption is closed to 100 kJ/mol (Ansari et al., 2014; Obi-Egbedi and Obot, 2011). As shown in Table 9, the inhibitor molecules tend to be physically adsorbed when the concentration of *PPE* is low, and they tend to undergo mixed adsorption dominated by physical adsorption at higher *PPE* concentrations.

3.10. Influence of test methods on adsorption mode

A comparison of the effects of the test methods, i.e. PDP, EIS and mass loss, on η value of the *PPE* inhibitor at 25 °C is presented in Fig. 14. The variation law of η with *PPE* concentration is hardly affected by the test methods. However, the η value for different test methods is also different, and generally in the order as PDP < EIS < mass loss. Also, the difference between the EIS and mass loss is small.

The adsorption of *PPE* on the surface of mild steel at room temperature did not follow the El-Awady and Temkin isotherms, thus the influence of the test methods was only examined in the case of the Langmuir isotherm, as shown in Fig. 15. The corresponding thermodynamic parameters are presented in Table 10. The correlation coefficient for three fitting lines is very close to one. The ΔG_{ads} value by the three methods is exceedingly similar. Moreover, difference in the K_{ads} value is unobvious. Therefore, it is concluded that the corrosion methods of PDP, EIS and mass loss have minimal effect on the evaluation of adsorption behaviour for *PPE*.

3.11. UV–vis and FT-IR spectra

When a molecule or ion absorbs radiation in the UV–vis region of the electromagnetic spectrum, the valence electrons

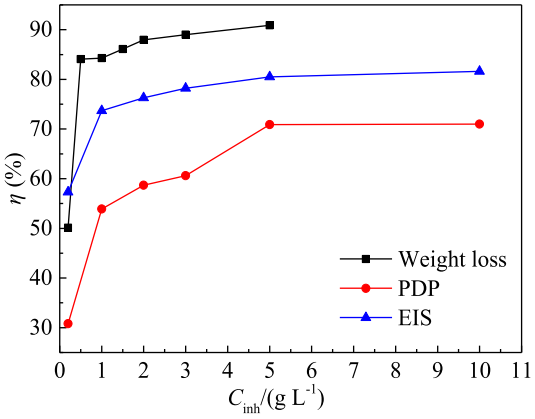

Fig. 14 Effect of the test methods on η value for *PPE*.

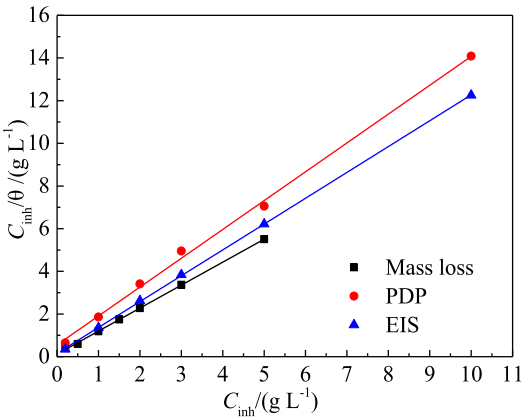

Fig. 15 Effect of test methods on the Langmuir isotherm.

and the orbital electrons will participate in energy level transitions thus generating the UV–vis absorption spectrum. The molecular composition can be qualitatively and semi-quantitatively analysed using UV–vis spectrophotometry. There are many organic molecules in plant extracts and the π-electrons of the compounds with conjugated structure readily absorbed UV–vis radiation to produce characteristic absorption peaks. Therefore, the structural characteristics of organic molecules with heteroatom non-ligand electrons and π-electrons in double bonds can be studied by UV–vis spectrophotometry (Pal et al., 2019; Singh et al., 2020). The UV–vis spectra for a 1.0 mol/L H_3PO_4 solution containing 5.0 g/L *PPE* before and after corrosion of mild steel are shown in Fig. 16.

As shown in Fig. 16, the absorption bands at 196 nm, 221 nm and 283 nm before immersion are due to the π-π* transition of C═C bonds in the aromatic rings. This indicates that the aromatic compounds, which contain unsaturated bonds with π-electron groups in *PPE*, are of the conjugated closed system type. The absorption band at 331 nm before immersion is due to the n-π* transition of C═O bonds in carbonyl compounds. It indicates that the extracts contain compounds having unsaturated bonds with n-electron groups (Caio et al., 2019; Chung et al., 2020; Saxena et al., 2018; Singh et al., 2020). After immersion and corrosion, the wavelengths of the above three absorption bands, corresponding to the π-π* transitions of C═C bond in the aromatic ring, are blue-shifted to 193 nm, 220 nm and 275 nm, respectively. The absorption bands related to the n-π* transitions of the C═O bonds in carbonyl compounds almost disappear. It can thus be concluded that both the C═C bonds and the carbonyl groups in *PPE* reacted with iron ions and formed the protection film on the surface of mild steel (Caio et al., 2019; Chung et al., 2020; Saxena et al., 2018; Singh et al., 2020).

Given the complex composition of *PPE*, FT-IR spectroscopy is needed to reveal the specific chemical bonds and functional groups of the active components. The FT-IR spectra of *PPE* and the *PPE* film which formed on the surface of the mild steel are presented in Fig. 17. Clearly, the positions of the absorption bands for the two spectra are quite similar, further confirming the adsorption of *PPE* on mild steel.

As shown in Fig. 17a, the broad absorption band at 3460 cm^{-1} corresponds to the stretching vibration of O─H (Alibakhshi et al., 2018; Bahlakeh et al., 2019; Ji et al., 2015;

Table 10 Effect of test methods on the parameters of the Langmuir isotherm for *PPE*.

Test method	Correlation coefficient (R^2)	Intercept	Slope	K_{ads}(L g^{-1})	ΔG_{ads}(kJ mol^{-1})
Mass loss	1.000	0.122	1.07	8.2	−22.1
PDP	0.999	0.237	1.35	4.3	−20.5
EIS	1.000	0.158	1.21	6.3	−21.4

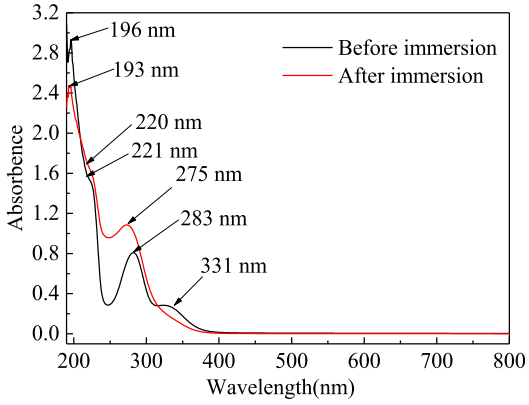

Fig. 16 UV–vis spectra for 1.0 mol/L H_3PO_4 solution containing 5.0 g/L *PPE* before and after steel corrosion.

Qiang et al., 2018). The strong absorption band at 2929 cm^{-1} is due to the stretching vibration of the saturated C—H bond. The strong and sharp absorption band at 1615 cm^{-1} is due to the stretching vibrations of C═C and C═O in the aromatic ring conjugation system. It should be noted that the large conjugation effect of C═O and C═C in the structure of flavonoids makes the absorption peak of C═O move to a low wave number, overlapping with the absorption band region for C═C (Byrne et al., 2020; Rahim et al., 2007; Snihirova et al., 2016). The absorption band at 1411 cm^{-1} is related to the bending vibration of the C—H bond in —CH_2 and the symmetric stretching vibration of COOH in the carboxyl group. The absorption band at 1367 cm^{-1} is due to the bending vibration of the C—H bond in —CH_3 (Alibakhshi et al., 2018; Bahlakeh et al., 2019; Ji et al., 2015; Qiang et al., 2018). The absorption bands at 1256 cm^{-1} and 1038 cm^{-1} are due to the stretching vibrations of the C—O bond in aromatic ethers and fatty ethers, respectively. The absorption peaks in the range 1600–1000 cm^{-1} may be the skeleton vibration region of the benzene ring or hetero-aromatic ring. The absorption band below 1000 cm^{-1} is due to the bending vibration of the C-H bond in the benzene ring or hetero-aromatic ring (Alibakhshi et al., 2018; Bahlakeh et al., 2019; Ji et al., 2015; Qiang et al., 2018). The results show that *PPE* contains —OH, C—O, C═O, C═C, —CH_2, —CH_3, benzene ring, hetero-aromatic ring and other functional groups. Therefore, *PPE* contains a mixture of polar organic groups (—OH, C—O, C═O, C═C and hetero-aromatic rings) and non-polar organic groups (—CH_2, —CH_3, benzene ring).

Compared with the FT-IR spectrum in Fig. 17a, the intensity of the absorption band for the *PPE* film on the mild steel surface in Fig. 17b is relatively weak. This can be attributed to the interaction between the *PPE* inhibitor and mild steel, as a result of the formation of the adsorbed film on the surface (Caio et al., 2019; Bahlakeh et al., 2019). This is consistent with the results for the UV–vis spectra.

According to the literatures (Sun et al., 2017; Yee et al., 2020), the main components in *Pomelo* peel include flavonoids, sterols, fatty acids, sugars and limonin. Flavonoids are the general term for a class of phenolic compounds with the C6-C3-C6 structure, and are widely distributed in the plant kingdom in the form of free aglycones or glycosides (Byrne et al., 2020; Rahim et al., 2007; Snihirova et al., 2016). The basic structure of flavonoids is shown in Fig. 18 (Mhiri et al., 2016; Toledo-Guillén et al., 2010; Zhang and Zhao, 2018).

The main flavonoids in *Pomelo* peel are naringin, neohesperidin, rutin and other dihydroflavones, in which naringin accounts for more than 80%. The structural formula of naringin in *PPE* is given in Fig. 19. There are active groups such as oxygen-containing hetero-cycles, hydroxyl groups and carbonyl groups in the molecular structure of naringin. Liu (2017) reported that the contents of the active components in *PPE* were as follows: 16.7% ketones, 7.9% alcohols, 21.9% acids and 49.7% lipids.

In the case of ketones, the main component groups include oxygen-containing hetero-cycles and the C═O unsaturated

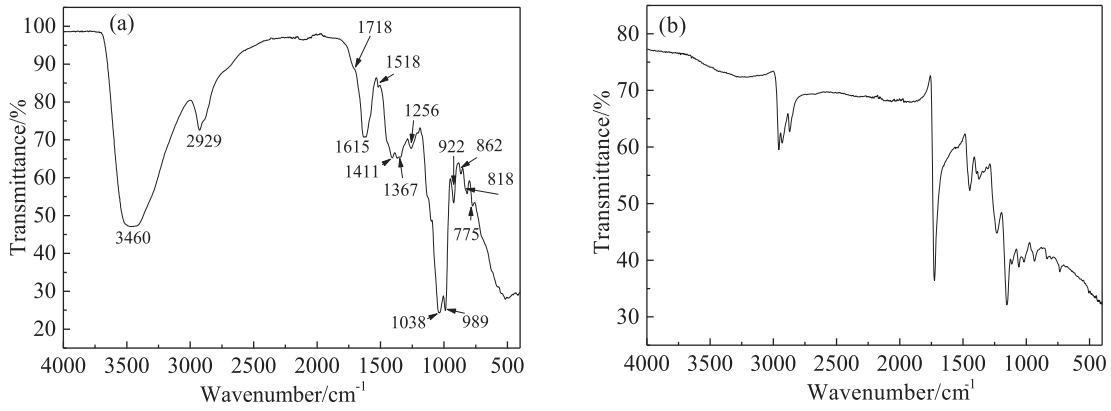

Fig. 17 FT-IR spectra for (a) *PPE* and (b) *PPE* film on mild steel surface.

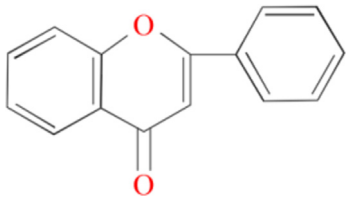

Fig. 18 Basic structure of flavonoids.

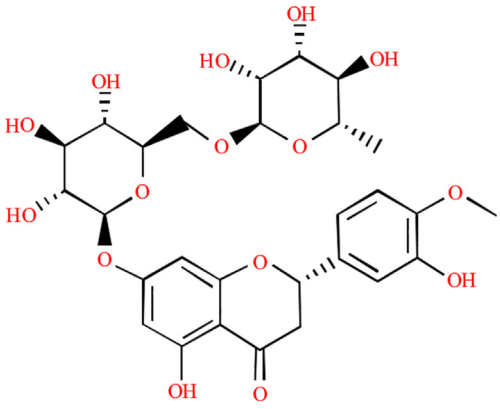

Fig. 19 Structural formula of naringin in *PPE*.

bonds. The basic structural formula for organic acids is RCOOH and organic acids possess carboxyl functional groups —COOH. In the case of alcohols, hydroxyl groups —OH are prevalent.

The UV–vis spectra reveal that *PPE* contains carbonyl compounds. The FT-IR spectra indicate that *PPE* contains hydroxyl, carbonyl and keto compounds. It is speculated that the inhibition mechanism of *PPE* for mild steel in 1.0 mol/L H_3PO_4 solution may depend on the following three adsorption modes (Bahlakeh et al., 2019; Caio et al., 2019; Hamdani et al., 2015): (1) Physical adsorption: the active polar groups are protonated in H_3PO_4 solution and create excess positive charge, which results in the adsorption of *PPE* on the metal surface due to the electrostatic attraction with the negatively charged surface of mild steel. (2) Chemical adsorption: there are unpaired electrons in the oxygen-containing hetero-cycles in the ketone carbonyl groups and the C and O atoms in C═O unsaturated bonds, which are able to form chelates with iron ions or donate electrons to the empty 3*d* orbitals of iron, thus forming coordination bonds. (3) Mixed adsorption: this is an adsorption process that features the characteristics of both physical adsorption and chemical adsorption as outlined above.

4. Conclusion

Detailed studies have been performed on the use of *PPE* as a green and renewable corrosion inhibitor for mild steel in 1.0 mol/L H_3PO_4 solution. The main conclusions are as follows:

- The corrosion rate for mild steel decreased with the increase in the *PPE* concentration ranged from 0 g/L to 5.0 g/L, but increased with the medium temperature ranged from 25 °C to 55 °C.
- *PPE* inhibits the corrosion of mild steel through the "geometric coverage" effect. *PPE* functions as a mixed corrosion inhibitor and confers on mild steel a long-term and highly efficient corrosion inhibition.
- The adsorption isotherm for *PPE* is affected by the temperature of the corrosion medium. For mild steel at 25, 35, 45 and 55 °C, the *PPE* obeys the Langmuir isotherm with a monolayer adsorption film. But it also follows the El-Awady and Temkin isotherms at the last three higher temperatures. One extract molecule can replace multiple water molecules, but repulsive forces act between the extract molecules.
- The test methods of mass loss, PDP and EIS have a minimal effect on the inhibition efficiency, and almost have no effect on the adsorption isotherm and thermodynamic parameters.
- The adsorption mode for *PPE* is influenced by the temperature of the corrosion medium and the *PPE* concentration. At 25 °C and at higher concentrations of the extract, *PPE* tends to undergo a mixed adsorption dominated by physical adsorption. Otherwise, physical adsorption is prevalent.
- FTIR and UV–vis spectra confirm an adsorption of *PPE* matters on the mild steel surface. The adsorption mechanism for *PPE* is controlled by the protonation of the active polar groups in the inhibitor molecules and the formation of chelates or coordination bonds with iron ions via the oxygen-containing hetero-cycles and C═O unsaturated bonds in naringin.

Declaration of Competing Interest

The authors declare that they have no known competing financial interests or personal relationships that could have appeared to influence the work reported in this paper.

Acknowledgment

This work was supported by the Natural Science Foundation of Fujian Province (Nos. 2020J01291 and 2020J01059), and the National Natural Science Foundation of China (No. 51778247).

References

Alibakhshi, E., Ramezanzadeh, M., Bahlakeh, G., Ramezanzadeh, B., Mahdavian, M., Motamedi, M., 2018. *Glycyrrhiza glabra* leaves extract as a green corrosion inhibitor for mild steel in 1 M hydrochloric acid solution: Experimental, molecular dynamics, Monte Carlo and quantum mechanics study. J. Mol. Liq. 255, 185–198.

Alrefaee, S.H., Rhee, K.Y., Verma, C., Quraishi, M.A., Ebenso, E.E., 2020. Challenges and advantages of using plant extract as inhibitors in modern corrosion inhibition systems: Recent advancements. J. Mol. Liq. 114666.

Anaee, R.A., Tomi, I.H.R., Abdulmajeed, M.H., Naser, S.A., Kathem, M.M., 2019. Expired Etoricoxib as a corrosion inhibitor for steel in acidic solution. J. Mol. Liq. 279, 594–602.

Ansari, K.R., Quraishi, M.A., Singh, A., 2014. Schiff's base of pyridyl substituted triazoles as new and effective corrosion inhibitors for mild steel in hydrochloric acid solution. Corros. Sci. 79, 5–15.

Anupama, K.K., Ramya, K., Shainy, K.M., Joseph, A., 2015. Adsorption and electrochemical studies of *Pimenta dioica* leaf

extracts as corrosion inhibitor for mild steel in hydrochloric acid. Mater. Chem. Phys. 167, 28–41.
Aslam, J., Aslam, R., Alrefaee, S.H., Mobin, M., Aslam, A., Parveen, M., Hussain, C.M., 2020. Gravimetric, electrochemical, and morphological studies of an isoxazole derivative as corrosion inhibitor for mild steel in 1M HCl. Arab. J. Chem. 13, 7744–7758.
Bahlakeh, G., Ramezanzadeh, B., Dehghani, A., Ramezanzadeh, M., 2019. Novel cost-effective and high-performance green inhibitor based on aqueous *Peganum harmala* seed extract for mild steel corrosion in HCl solution: Detailed experimental and electronic/atomic level computational explorations. J. Mol. Liq. 283, 174–195.
Belghiti, M.E., Echihi, S., Dafali, A., Karzazi, Y., Bakasse, M., Elalaoui-Elabdallaoui, H., Olasunkanmi, L.O., Ebenso, E.E., Tabyaoui, M., 2019. Computational simulation and statistical analysis on the relationship between corrosion inhibition efficiency and molecular structure of some hydrazine derivatives in phosphoric acid on mild steel surface. Appl. Surf. Sci. 491, 707–722.
Benarioua, M., MihiNora, A., Bouzeghaia, N., Naoun, M., 2019. Mild steel corrosion inhibition by *Parsley (Petroselium sativu*m) extract in acidic media. Egypt. J. Pet. 28, 155–159.
Boudalia, M., Fernández-Domene, R.M., Tabyaoui, M., Bellaouchou, A., Guenbour, A., Gloopía-Antón, J., 2019. Green approach to corrosion inhibition of stainless steel in phosphoric acid of Artemesia herba albamedium using plant extract. J. Mater. Res. Technol. 8 (6), 5763–5773.
Byrne, C., Selmi, G.J., Alessandro, O.D., Deyá, C., 2020. Study of the anticorrosive properties of "quebracho colorado" extract and its use in a primer for aluminum1050. Prog. Org. Coat. 148, 105827.
Caio, M.F., Thayssa, D.S.F.F., Escarpini, D.S.N., Shewry, D.M.R.T., Rafael, G., Ricardo, M.B., Guilherme, M., Alessandra, L.V., Eduardo, A.P., 2019. *Ircinia strobilina* crude extract as corrosion inhibitor for mild steel in acid medium. Electrochim. Acta 312, 137–148.
Cao, C.N., 2008. Principles of Electrochemistry of Corrosion. Chemical Industry Press, Beijing.
Cao, C.N., Zhang, J.Q., 2002. An Introduction to Electrochemical Impedance Spectroscopy. Science Press, Beijing.
Chung, I.M., Malathy, R., Priyadharshini, R., Hemapriya, V., Kim, S. H., Prabakaran, M., 2020. Inhibition of mild steel corrosion using *Magnolia kobus* extract in sulphuric acid medium. Mater. Today Commun. 25, 101687.
Dehghani, A., Bahlakeh, G., Ramezanzadeh, B., Ramezanzadeh, M., 2020. Potential role of a novel green eco-friendly inhibitor in corrosion inhibition of mild steel in HCl solution: Detailed macro/micro-scale experimental and computational explorations. Constr. Build. Mater. 245, 118464.
Dehghani, A., Bahlakeh, G., Ramezanzadeh, B., Ramezanzadeh, M., 2019. Potential of *Borage* flower aqueous extract as an environmentally sustainable corrosion inhibitor for acid corrosion of mild steel: Electrochemical and theoretical studies. J. Mol. Liq. 277, 895–911.
Deyab, M.A., Abd El-Rehim, S.S., 2012. On surfactant-polymer association and its effect on the corrosion behavior of carbon steel in cyclohexane propionic acid. Corros. Sci. 65, 309–316.
Deyab, M.A., Abd El-Rehim, S.S., 2013. Influence of polyethylene glycols on the corrosion inhibition of carbon steel in butyric acid solution: weight loss, EIS and theoretical studies. Int. J. Electrochem. Sci. 8, 12613–12627.
Divya, P., Subhashini, S., Prithiba, A., Rajalakshmi, R., 2019. *Tithonia diversifolia* flower extract as green corrosion inhibitor for mild steel in acid medium. Mater. Today Proc. 18, 1581–1591.
Dkhireche, N., Galai, M., Ouakki, M., Rbaa, M., Ech-chihbi, E., Lakhrissi, B., Touhami, M.E., 2020. Electrochemical and theoretical study of newly quinoline derivatives as a corrosion inhibitors adsorption on mild steel in phosphoric acid media. Inorg. Chem. Commun. 121, 108222.
Ech-chihbi, E., Nahlé, A., Salim, R., Benhiba, F., Moussaif, A., El-Hajjaji, F., Oudda, H., Guenbour, A., Taleb, M., Warad, I., Zarrouk, 2020. Computational, MD simulation, SEM/EDX and experimental studies for understanding adsorption of benzimidazole derivatives as corrosion inhibitors in 1.0 M HCl solution. J. Alloy. Comp. 844, 155842.
El-Etre, A.Y., Abdallah, M., 2000. Natural honey as corrosion inhibitor for metals and alloys. II. C-steel in high saline water. Corros. Sci. 42, 731–738.
El-Ibrahimi, B., Jmiai, A., Bazzi, L., El Issami, S., 2020. Amino acids and their derivatives as corrosion inhibitors for metals and alloys. Arab. J. Chem. 13, 740–771.
ElKacimi, Y., ElBakri, H., Alaoui, K., Touir, R., Galai, M., Ebn Touhami, M., Doubi, M., 2020. Synergistic effect study of Cetyl Trimethyl Ammonium Bromide with iodide ions at low concentration for mild steel corrosion in 5.0 M HCl medium. Chem. Data Collections 30, 100558.
Fadhil, A.A., Khadom, A.A., Ahmed, S.K., Liu, H., Fu, C., Mahood, H.B., 2020. *Portulaca grandiflora* as new green corrosion inhibitor for mild steel protection in hydrochloric acid: Quantitative, electrochemical, surface and spectroscopic investigations. Surf. Interf. 20, 100595.
Fang, L.P., Zeng, W.B., Xu, L., Huang, L.Z., 2020. Green rusts as a new solution to sequester and stabilize phosphate in sediments under anoxic conditions and their implication for eutrophication control. Chem. Eng. J. 388, 124198.
Fateh, A., Aliofkhazraei, M., Rezvanian, A.R., 2020. Review of corrosive environments for copper and its corrosion inhibitors. Arab. J. Chem. 13, 481–544.
Faustin, M., Maciuk, A., Salvin, P., Roos, C., Lebrini, M., 2015. Corrosion inhibition of C38 steel by alkaloids extract of *Geissospermum* leaves in 1 M hydrochloric acid: electrochemical and phytochemical studies. Corros. Sci. 92, 287–300.
Faydy, M.E., Lakhrissi, B., Jama, C., Zarrouk, A., Olasunkanmi, L. O., Ebenso, E.E., Bentiss, F., 2020. Electrochemical, surface and computational studies on the inhibition performance of some newly synthesized 8-hydroxyquinoline derivatives containing benzimidazole moiety against the corrosion of carbon steel in phosphoric acid environment. J. Mater. Res. Technol. 9 (1), 727–748.
Fayomi, O.S.I., Fayomi, J., Elemike, E.E., 2018. Data on anti-corrosion characteristics of eco-friendly inhibitive extract on the hot corrosion degradation trend of A6063 aluminum alloy in 1.0 M HCl solution. Data in Brief 19, 2468–2476.
Ferreira, E.S., Giacomelli, C., Giacomelli, F.C., Spinelli, A., 2004. Evaluation of inhibitor effect of L-ascorbic acid on the corrosion of mild steel. Mater. Chem. Phys. 83, 129–134.
Gao, X., Zhao, C., Lu, H., Gao, F., Ma, H., 2014. Influence of phytic acid on the corrosion behavior of iron under acidic and neutral conditions. Electrochim. Acta 150, 188–196.
Garai, S., Garai, S., Jaisankar, P., Singh, J.K., Elango, A., 2012. A comprehensive study on crude methanolic extract of *Artemisia pallens (Asteraceae*) and its active component as effective corrosion inhibitors of mild steel in acid solution. Corros. Sci. 60, 193–204.
Gunasekaran, G., Chauhan, L.R., 2004. Eco friendly inhibitor for corrosion inhibition of mild steel in phosphoric acid medium. Electrochim. Acta 49, 4387–4395.
Hamdani, N.E., Fdil, R., Tourabi, M., Jama, C., Bentiss, F., 2015. Alkaloids extract of *retama monosperma (L.) boiss.* seeds used as novel eco-friendly inhibitor for carbon steel corrosion in 1 M HCl solution: Electrochemical and surface studies. Appl. Surf. Sci. 357, 1294–1305.
Harb, M.B., Abubshait, S., Etteyeb, N., Kamoun, M., Dhouib, A., 2020. Olive leaf extract as a green corrosion inhibitor of reinforced concrete contaminated with seawater. Arab. J. Chem. 13, 4846–4856.
Hassan, K.H., Khadom, A.A., Kurshed, N.H., 2016. *Citrus aurantium* leaves extracts as a sustainable corrosion inhibitor of mild steel in sulfuric acid. S. Afr. J. Chem. Eng. 22, 1–5.
Hassannejad, H., Nouri, A., 2018. Sunflower seed hull extract as a novel green corrosion inhibitor for mild steel in HCl solution. J. Mol. Liq. 254, 377–382.

Hu, K., Zhuang, J., Ding, J., Ma, Z., Wang, F., Zeng, X., 2017. Influence of biomacromolecule DNA corrosion inhibitor on carbon steel. Corros. Sci. 125, 68–76.

Hu, Z., Meng, Y., Ma, X., Zhu, H., Li, J., Li, C., Cao, D., 2016. Experimental and theoretical studies of benzothiazole derivatives as corrosion inhibitors for carbon steel in 1M HCl. Corros. Sci. 112, 563–575.

Hussin, M.H., Kassim, M.J., Razali, N.N., Dahon, N.H., Nasshorudin, D., 2016. The effect of *Tinospora crispa* extracts as a natural mild steel corrosion inhibitor in 1 M HCl solution. Arab. J. Chem. 9, 616–624.

Ismail, A.S., Farag, A.A., 2020. Experimental, theoretical and simulation studies of extracted crab waste protein as a green polymer inhibitor for carbon steel corrosion in 2 M H_3PO_4. Surf. Interfaces 19, 100483.

Ituen, E., Akaranta, O., James, A., Sun, S.Q., 2017. Green and sustainable local biomaterials for oilfield chemicals: *Griffonia simplicifolia* extract as steel corrosion inhibitor in hydrochloric acid. Sustain. Mater. Technol. 11, 12–18.

Ji, G., Anjum, S., Sundaram, S., Prakash, R., 2015. *Musa paradisica* peel extract as green corrosion inhibitor for mild steel in HCl solution. Corros. Sci. 90, 107–117.

Jmiai, A., El-Ibrahimi, B., Tara, A., Chadili, M., Issami, S.E., Jbara, O., Khallaayoun, A., Bazzi, L., 2018. Application of *Zizyphus lotuse* - pulp of jujube extract as green and promising corrosion inhibitor for copper in acidic medium. J. Mol. Liq. 268, 102–113.

Jyothi, S., Ravichandran, J., 2014. Corrosion inhibition of mild steel in sulphuric acid using *Luffa aegyptiaca* leaves extract. Acta Metall. Sin. (Engl. Lett.) 27, 969–980.

Khadom, A.A., Abd, A.N., Ahmed, N.A., 2018. *Xanthium strumarium* leaves extracts as a friendly corrosion inhibitor of low carbon steel in hydrochloric acid: Kinetics and mathematical studies. S. Afr. J. Chem. Eng. 25, 13–21.

Khaled, K.F., 2003. The inhibition of benzimidazole derivatives on corrosion of iron in 1 M HCl solutions. Electrochim. Acta 48, 2493–2503.

Khan, G., Basirun, W.J., Kazi, S.N., Ahmed, P., Magaji, L., Ahmed, S.M., Khan, G.M., Rehman, M.A., 2017. Electrochemical investigation on the corrosion inhibition of mild steel by *Quinazoline Schiff* base compounds in hydrochloric acid solution. J. Colloid Interf. Sci. 502, 134–145.

Li, X.H., Deng, S.D., Fu, H., Zhao, N., Li, Y.X., Mu, G.N., 2009. Corrosion inhibiton of cresol red for cold rolled steel in phosphoric acid solution. Corros. Sci. Protect. Technol. 21 (4), 354–357.

Li, X.H., Deng, S.D., 2020. Synergistic inhibition effect of walnut green husk extract and potassium iodide on the corrosion of cold rolled steel in trichloroacetic acid solution. J Mater. Res. Technol. 9, 15604–15620.

Liu, S.J., 2017. Performance of Pomelo Peel Extract as Corrosion Inhibitor for Acid Pickling. Southwest Petroleum University, Chengdu.

Ma, H., Cheng, X., Li, G., Chen, S., Quan, Z., Zhao, S., Niu, L., 2000. The influence of hydrogen sulfide on corrosion of iron under different conditions. Corros. Sci. 42, 1669–1683.

Messali, M., Lgaz, H., Dassanayake, R., Salghi, R., Jodeh, S., Abidi, N., Hamed, O., 2017. Guar gum as efficient non-toxic inhibitor of carbon steel corrosion in phosphoric acid medium: Electrochemical, surface, DFT and MD simulations studies. J. Mol. Struct. 1145, 43–54.

Mhiri, N., Veys-Renaux, D., Rocca, E., Ioannou, I., Boudhrioua, N. M., Ghoul, M., 2016. Corrosion inhibition of carbon steel in acidic medium by orange peel extract and its main antioxidant compounds. Corros. Sci. 102, 55–62.

Mobin, M., Basik, M., Aslam, J., 2019. Pineapple stem extract (*Bromelain*) as an environmental friendly novel corrosion inhibitor for low carbon steel in 1 M HCl. Measurement 134, 595–605.

Mourya, P., Banerjee, S., Singh, M.M., 2014. Corrosion inhibition of mild steel in acidic solution by *Tagetes erecta (Marigold* flower) extract as a green inhibitor. Corros. Sci. 85, 352–363.

Nadi, I., Belattmania, Z., Sabour, B., Reani, A., Sahibed-dine, A., Jama, C., Bentiss, F., 2019. *Sargassum muticum* extract based on alginate biopolymer as a new efficient biological corrosion inhibitor for carbon steel in hydrochloric acid pickling environment: Gravimetric, electrochemical and surface studies. Int. J. Biol. Macromol. 141, 137–149.

Nathiya, R.S., Raj, V., 2017. Evaluation of *Dryopteris cochleata* leaf extracts as green inhibitor for corrosion of aluminium in 1 M H_2SO_4. Egypt. J. Pet. 26, 313–323.

Nathiya, R.S., Perumal, S., Murugesan, V., Raj, V., 2019. Evaluation of extracts of *Borassus flabellifer* dust as green inhibitors for aluminium corrosion in acidic media. Mater. Sci. Semicon. Proc. 104, 104674.

Nikpour, S., Ramezanzadeh, M., Bahlakeh, G., Ramezanzadeh, B., Mahdavian, M., 2019. *Eriobotrya japonica lindl* leaves extract application for effective corrosion mitigation of mild steel in HCl solution: Experimental and computational studies. Constr. Build. Mater. 220, 161–176.

Obi-Egbedi, N.O., Obot, I.B., Umoren, S.A., 2015. *Spondias mombin L.* as a green corrosion inhibitor for aluminium in sulphuric acid: Correlation between inhibitive effect and electronic properties of extracts major constituents using density functional theory. Arab. J. Chem. 5, 361–373.

Obi-Egbedi, N.O., Obot, I.B., 2011. Inhibitive properties, thermodynamic and quantum chemical studies of alloxazine on mild steel corrosion in H_2SO_4. Corros. Sci. 53, 263–275.

Oguzie, E.E., Enenebeaku, C.K., Akalezi, C.O., Okoro, S.C., Ayuk, A. A., Ejike, E.N., 2010. Adsorption and corrosion-inhibiting effect of *Dacryodis edulis* extract on low carbon steel corrosion in acidic media. J. Colloid Interf. Sci. 349, 283–292.

Outirite, M., Lagrenée, M., Lebrini, M., Traisnel, M., Jama, C., Vezin, H., Bentiss, F., 2010. AC impedance, X-ray photoelectron spectroscopy and density functional theory studies of 5-bis(n-pyridyl)-1,2,4-oxadiazoles as efficient corrosion inhibitors for carbon steel surface in hydrochloric acid solution. Electrochim. Acta 55, 1670–1681.

Pal, S., Lgaz, H., Tiwari, P., Chung, I.M., Ji, G., Prakash, R., 2019. Experimental and theoretical investigation of aqueous and methanolic extracts of *Prunus dulcis* peels as green corrosion inhibitors of mild steel in aggressive chloride media. J. Mol. Liq. 276, 347–361.

Popoola, L.T., 2019. Progress on pharmaceutical drugs, plant extracts and ionic liquids as corrosion inhibitors. Heliyon 5, 1–60.

Qian, B., Wang, J., Zheng, M., Hou, B., 2013. Synergistic effect of polyaspartic acid and iodide ion on corrosion inhibition of mild steel in H_2SO_4. Corros. Sci. 75, 184–192.

Qiang, Y.J., Zhang, S.T., Tan, B.C., Chen, S.J., 2018. Evaluation of *Ginkgo* leaf extract as an eco-friendly corrosion inhibitor of X70 steel in HCl solution. Corros. Sci. 133, 6–16.

Rahim, A.A., Rocca, E., Steinmetz, J., Kassim, M.J., Adnan, R., Ibrahim, M.S., 2007. Mangrove tannins and their flavanoid monomers as alternative steel corrosion inhibitors in acidic medium. Corros. Sci. 49, 402–417.

Raja, P.B., Sethuraman, M.G., 2008. Natural products as corrosion inhibitor for metals in corrosive media–A review. Mater. Lett. 62, 113–116.

Reis, F.M., De Melo, H.G., Costa, I., 2006. EIS investigation on Al 5052 alloy surface preparation for self-assembling monolayer. Electrochim. Acta 51, 1780–1788.

Saei, E., Ramezanzadeh, B., Amini, R., Kalajahi, M.S., 2017. Effects of combined organic and inorganic corrosion inhibitors on the nanostructure cerium based conversion coating performance on AZ31 magnesium alloy: Morphological and corrosion studies. Corros. Sci. 127, 186–200.

Satapathy, A.K., Gunasekaran, G., Sahoo, S.C., Amit, K., Rodrigues, P.V., 2009. Corrosion inhibition by *Justicia gendarussa* plant extract in hydrochloric acid solution. Corros. Sci. 51, 2848–2856.

Saxena, A., Prasad, D., Haldhar, R., Singh, G., Kumar, A., 2018. Use of *Saraca ashoka* extract as green corrosion inhibitor for mild steel in 0.5 M H_2SO_4. J. Mol. Liq. 258, 89–97.

Shih, H., Mansfeld, F., 1989. A fitting procedure for impedance data of systems with very low corrosion rates. Corros. Sci. 29, 1235–1240.

Shukla, S.K., Ebenso, E.E., 2011. Corrosion inhibition, adsorption behavior and thermodynamic properties of streptomycin on mild steel in hydrochloric acid medium. Int. J. Electrochem. Sci. 6, 3277–3329.

Sin, H.L.Y., Rahim, A.A., Gan, C.Y., Saad, B., Salleh, M.I., Umeda, M., 2017. *Aquilaria subintergra* leaves extracts as sustainable mild steel corrosion inhibitors in HCl. Measurement 109, 334–345.

Singh, A., Xia, D., Ituen, E., Ansari, K., Quraishi, M.A., Kaya, S., Lin, Y., 2020. Tobacco extracted from the discarded cigarettes as an inhibitor of copper and zinc corrosion in an ASTM standard D1141–98(2013) artificial seawater solution. J. Mater. Res. Technol. 9, 5161–5173.

Singh, M.R., Gupta, P., Gupta, K., 2019. The litchi (*Litchi Chinensis*) peels extract as a potential green inhibitor in prevention of corrosion of mild steel in 0.5 M H_2SO_4 solution. Arab. J. Chem. 12, 1035–1041.

Singh, P., Quraishi, M.A., 2016. Corrosion inhibition of mild steel using Novel Bis Schiff's Bases as corrosion inhibitors: Electrochemical and Surface measurement. Measurement 86, 114–124.

Snihirova, D., Lamaka, S., Taheri, P., Mol, J., Montemor, M., 2016. Comparison of the synergistic effects of inhibitor mixtures tailored for enhanced corrosion protection of bare and coated AA2024-T3. Surf. Coat. Technol. 303, 342–351.

Solmaz, R., 2010. Investigation of the inhibition effect of 5-((E)-4-phenylbuta-1,3-dienylideneamino)-1,3,4- thiadiazole-2-thiol *Schiff base* on mild steel corrosion in hydrochloric acid. Corros. Sci. 52, 3321–3330.

Solomon, M.M., Umoren, S.A., 2015. Electrochemical and gravimetric measurements of inhibition of aluminum corrosion by poly (methacrylic acid) in H2SO4 solution and synergistic effect of iodide ions. Measurement 76, 104–116.

Souza, F.S., Spinelli, A., 2009. *Caffeic* acid as a green corrosion inhibitor for mild steel. Corros. Sci. 51, 642–649.

Sun, Z.P., Singh, A., Xu, X.H., Chen, S.S., Liu, W.Y., Lin, Y.H., 2017. Inhibition effect of *Pomelo* peel extract for N80 steel in 3.5% NaCl saturated with CO_2 solution. Res. Chem. Intermediat. 43, 6719–6736.

Taha, A.A., Abouzeid, F.M., Elsadek, M.M., Habib, F.M., 2020. Effect of methanolic plant extract on copper electro-polishing in ortho-phosphoric acid. Arab. J. Chem. 13, 6606–6625.

Talkhan, A.G., Benamor, A., Nasser, M.S., Qiblawey, H., El-Tayeb, S.A., El-Marsafy, S.M., 2019. Corrosion study of carbon steel in CO_2 loaded solution of N-methyldiethanolamine and l-arginine mixtures. J. Electroanal. Chem. 837, 10–21.

Toledo-Guillén, A.R., Higuera-Ciapara, I., Gloopía-Navarrete, G., de la Fuente, J.C., 2010. Extraction of bioactive flavonoid compounds from orange (*Citrus sinensis*) peel using supercritical CO_2. J. Biotechnol. 150, 313–314.

Uwah, I.E., Okafor, P.C., Ebiekpe, V.E., 2013. Inhibitive action of ethanol extracts from *Nauclea latifolia* on the corrosion of mild steel in H_2SO_4 solutions and their adsorption characteristics. Arab. J. Chem. 6, 285–293.

Verma, C., Ebenso, E.E., Bahadur, I., Quraishi, M.A., 2018. An overview on plant extracts as environmental sustainable and green corrosion inhibitors for metals and alloys in aggressive corrosive media. J. Mol. Liq. 266, 577–590.

Wang, Q.H., Tan, B.C., Bao, H.B., Xie, Y.T., Mou, Y.X., Li, P.C., Chen, D.B., Shi, Y.W., Li, X.M., Yang, W.J., 2019. Evaluation of *Ficus tikoua* leaves extract as an eco-friendly corrosion inhibitor for carbon steel in HCl media. Bioelectrochem. 128, 49–55.

Xhanari, K., Finšgar, M., 2019. Organic corrosion inhibitors for aluminum and its alloys in chloride and alkaline solutions: A review. Arab. J. Chem. 12, 4646–4663.

Xu, X., Li, X.H., Deng, S.D., 2019. Synergistic inhibition effect of *Walnut Green Husk* extract and sodium dodecyl sulfate on cold rolled steel in H_3PO_4 solution. Surf. Technol. 48, 281–288.

Yaro, A.S., Khadom, A.A., Wael, R.K., 2013. Apricot juice as green corrosion inhibitor of mild steel in phosphoric acid. Alex. Eng. J. 52, 129–135.

Yee, Y.P., Saud, S.N., Hamzah, E., 2020. *Pomelo* peel extract as corrosion inhibitor for steel in simulated seawater and acidic mediums. J. Mater. Eng. Perform. 29, 2202–2215.

Zhang, C., Zhao, J.M., 2018. Inhibition effects of orange peel extract on the corrosion of Q235 steel in CO_2-saturated and CO_2/H_2S coexistent brine solutions. Res. Chem. Intermediat. 44, 1275–1293.